Available online at www.sciencedirect.com

ScienceDirect

Geochimica et Cosmochimica Acta 283 (2020) 22–39

Geochimica et Cosmochimica Acta

www.elsevier.com/locate/gca

Experimental measurement of $H_{2(aq)}$ solubility in hydrothermal fluids: Application to the Piccard hydrothermal field, Mid-Cayman Rise

Peter P. Scheuermann *, Yanlu Xing, Kang Ding, William E. Seyfried Jr.

University of Minnesota, Department of Earth and Environmental Sciences, 116 Church St. SE, Minneapolis, MN 55455, USA

Received 20 January 2020; accepted in revised form 19 May 2020; available online 29 May 2020

Abstract

In mid-ocean ridge hydrothermal systems the fluid redox state is controlled by oxidation of ferrous iron in the host rock and generation of aqueous hydrogen, $H_{2(aq)}$. A quantitative interpretation of redox state requires conversion of $H_{2(aq)}$ concentrations to H_2 fugacity, f H_2. Here we present the results of hydrothermal experiments that calibrate the f H_2-concentration relationship in saline hydrothermal fluids, $Y_{H_2\text{-Cl}}$. $H_{2(aq)}$ concentrations were measured between 400 and 500 °C, 210 and 510 bar, in both single-phase fluids and low-density vapors in the KCl-H_2O system. The assemblage hematite-magnetite was used to buffer f H_2. Values of $Y_{H_2\text{-Cl}}$ are well above unity and decrease as temperature increases. Along isotherms $Y_{H_2\text{-Cl}}$ decreases as the fluid density decreases. At 400 °C, 330 bar and 1000 mmol/kg KCl $Y_{H_2\text{-Cl}}$ is 316 bar/molal and decreases to 4 bar/molal at 500 °C, 400 bar and 33 mmol/kg KCl. In combination with previous determination of $H_2S_{(aq)}$ solubility at hydrothermal conditions, the data presented here permit calculation of the redox conditions of natural vent systems. Redox conditions calculated for the basalt-hosted Piccard hydrothermal field suggest amphibolite facies mineral assemblages are present at depth, consistent with the extremely hot temperatures (>500 °C) inferred from analysis of other aspects of vent fluid chemistry (e.g., Cl and SiO_2). Piccard may be the first location of active venting that records, through its composition, evidence for an alteration assemblage that had been previously observed only in fossilized submarine hydrothermal systems.

Keywords: Henry's law; Hydrothermal; Experiment; Phase separation; Piccard vent field

1. INTRODUCTION

In mid-ocean ridge (MOR) vent fluids, $H_{2(aq)}$ and $H_2S_{(aq)}$ serve as important indicators of subsurface lithology (Seyfried and Ding, 1995; Von Damm, 2000) as well as energy sources for unique chemosynthetic organisms (e.g., Anderson et al., 2017 and references therein). Fluids with $H_{2(aq)}$ concentrations less than $H_2S_{(aq)}$ have commonly been interpreted to reflect alteration of mafic rocks, while the inverse ($H_{2(aq)} > H_2S_{(aq)}$) is most often indicative of hydrothermal alteration of ultramafic rocks (Charlou et al., 2002; Schmidt et al., 2007; Seyfried et al., 2011). In order to most accurately differentiate between various styles of hydrothermal alteration, the measured concentrations of redox-dependent gases must be converted to a thermodynamic parameter such as fugacity or activity. Conversely, fugacity or activity must be converted to concentration in any calculation that aims to predict the concentration of a dissolved gas in equilibrium with a given mineral assemblage. To date, calculations involving redox-dependent gases in MOR settings have often been performed using the assumption that the activity coefficients for $H_{2(aq)}$ or

* Corresponding author.
E-mail address: scheu101@umn.edu (P.P. Scheuermann).

https://doi.org/10.1016/j.gca.2020.05.020
0016-7037/

$H_2S_{(aq)}$ are equal to that of $CO_{2(aq)}$ at the same pressure–temperature conditions (e.g., McCollom and Shock, 1998; Klein et al., 2009; Klein et al., 2013). Interpretations of natural processes based on such calculations are uncertain since it is well established that non-ideal behavior is unique to each dissolved gas (e.g., Drummond, 1981, Akinfiev and Diamond, 2003). For example, Drummond (1981) performed experiments at 350 °C, vapor saturation and showed that the $f\,H_2$-concentration relationship is 117 bar/molal in pure water and increases to 395 bar/molal in 6 molal NaCl-H_2O. The deviation between $f\,H_2S$ and concentration is 27–88 bar/molal over the same range of conditions, while that for CO_2 is 48–240 bar/molal (Drummond, 1981). These data also highlight that, for a given gas, the deviation between fugacity and concentration is a complex function of pressure, temperature and dissolved salt concentration.

Measurements of pressure, temperature, and dissolved chloride in vent fluids at numerous sites on the seafloor attest to the variability of these parameters in natural systems. Hydrothermal fluids have been measured venting at the seafloor between 75 and 400+ °C, 80 and 500 bar, corresponding to water depths of 800–5000 meters (Von Damm, 1995; German and Seyfried, 2014; Seyfried et al., 2015; McDermott et al., 2018). Measured Cl concentrations vary dramatically, from 32 mmol/kg in the aftermath of a volcanic eruption (Von Damm, 2000; Lilley et al., 2003), to almost 1000 mmol/kg, twice the concentration in seawater (Gallant and Von Damm, 2006). The large range in Cl concentrations is the result of complex processes involving phase separation in the NaCl-H_2O system (Von Damm, 1990). Consistent with the behavior of $H_{2(aq)}$ and $H_2S_{(aq)}$ solubility in experimental studies (e.g., Drummond 1981), measurements of natural fluid chemistry demonstrate a negative correlation between dissolved gases and Cl concentrations (Ding and Seyfried, 1992; Seewald et al., 2003; Foustoukos and Seyfried, 2005).

In addition to dissolved Cl concentration, fluid-mineral equilibria play an important role in determining $H_{2(aq)}$ and $H_2S_{(aq)}$ concentrations in MOR vent fluids. This is because, at hydrothermal conditions within the ocean crust, the primary mechanism for $H_{2(aq)}$ formation is the oxidation of ferrous iron in the host rock. This process can be represented through a generalized reaction such as

$$FeO + H_2O = Fe_2O_3 + H_{2(aq)} \quad (1)$$

$H_2S_{(aq)}$ formation can be represented by the reaction of sulfides with hydrothermal fluid:

$$FeS + 4\ H_2O = Fe_3O_4 + 3\ H_2S_{(aq)} + H_{2(aq)} \quad (2)$$

The relatively constant $H_{2(aq)}$ and $H_2S_{(aq)}$ concentrations issuing from individual vent sites over long periods (Von Damm, 1995; Von Damm et al., 1995; Von Damm, 2000) and the differences in the concentration of both gases between mafic and ultramafic hosted vent sites indicate the importance of fluid-mineral equilibria in MOR systems. The results of experimental studies also support the hypothesis that dissolved gas concentrations represent equilibrium with the host rock (Seyfried and Ding, 1995; Seyfried et al., 2002).

Given the importance of $H_{2(aq)}$ and $H_2S_{(aq)}$ as indicators of redox state of MOR vent fluids, the usefulness of experiments that measure $H_{2(aq)}$ and $H_2S_{(aq)}$ concentrations in well-constrained experimental systems cannot be overstated. However, few studies have systematically measured gas solubility in salt bearing aqueous fluids at requisite hydrothermal conditions, significantly hampering the calculation of $H_{2(aq)}$ and $H_2S_{(aq)}$ concentration or fugacity in thermodynamic models. In this study, we present new experimental data on the solubility of the assemblage hematite-magnetite coexisting with vapor–liquid and single-phase fluids (KCl-H_2O) between 400–500 °C and 215–510 bar. The experiments focused on measuring $H_{2(aq)}$ in solutions with a range of Cl concentrations in order to expand the range of pressures, temperatures and salt concentrations over which the $f\,H_2$-concentration relationship can be calculated. The new experimental data can be used with previous measurements of $H_2S_{(aq)}$ solubility to interpret subsurface alteration processes associated with fluids issuing from MOR vent systems. Here, we leverage the data to understand the alteration processes responsible for the unique $H_{2(aq)}/H_2S_{(aq)}$ concentration ratio observed at the mafic-hosted Piccard vent field (Mid-Cayman Rise), the deepest vent field yet discovered.

2. METHODS

2.1. Hydrothermal Reactor

Experiments were performed in a newly designed fixed volume (150 mL) hydrothermal reactor (Scheuermann et al., 2018). The reactor body and closure piece are constructed from Ti-6Al-2Sn-4Zr-2Mo (Ti6242), a high strength titanium alloy, while all capillary lines and high temperature adapters are made from grade 2 titanium. A 1/16″ Ti-sheathed type E (chromel-constantan) thermocouple monitors the fluid temperature inside the reactor. The thermocouple communicates with three external heating bands through an EZ Zone PM (Watlow Electric Manufacturing Co.) proportional-integral-derivative controller. Error in temperature is ±5 °C, as determined by testing of the thermocouple in a dry block probe calibrator (Omega Hot Point©). A Teledyne ISCO syringe pump controls the system pressure, up to a maximum of 517 bar. The syringe pump can automatically inject or withdraw fluid to maintain constant pressure during sampling. Due to the redox sensitive nature of the present experiment, the interior surface of the reactor was passivated with 20 wt% nitric acid (300 °C, 10 h) in order to form an inert $TiO_{2(s)}$ coating on all wetted surfaces, following the procedure outlined by Fowler et al. (2019). The reactor used in this study is identical to that used by Fowler et al. (2019). As part of their study, Fowler et al. (2019) injected a known amount of $H_{2(aq)}$ into a passivated Ti-alloy reactor at 300 °C, 300 bar and measured the concentration periodically over five days. Within error, there was no change in the dissolved $H_{2(aq)}$ concentration, indicating that after passivation the Ti-alloy does not participate in reactions involving $H_{2(aq)}$ (Fowler et al., 2019).

The newly designed reactor significantly increases the effectiveness with which high temperature experiments involving phase separation can be performed. Specifically, the fixed-volume design and connection to the ISCO syringe pump accommodate large changes in fluid volumes that accompany phase separation. The design of the sampling valves, however, does not allow fluids to be withdrawn with a 'quick-quench' method (e.g., Foustoukos and Seyfried, 2005) necessary to avoid precipitation of Fe-sulfides in the capillary tubing. For this reason, sulfide minerals were not included in the experiments to buffer $f\,H_2S$.

2.2. Experimental procedure

This study employs the well-known mineral buffer technique to control $f\,H_2$ as a function of pressure and temperature (e.g., Chou, 1978; Kishima and Sakai, 1984a). This technique relies on establishing equilibrium between well characterized minerals phases (see Sections 2.3 and 3) and the coexisting fluid. The hematite and magnetite crystals used for these experiments were natural samples and came from the University of Minnesota Department of Earth and Environmental Sciences mineral collection. The minerals were broken and sieved and the 1–2 millimeter size fraction was retained. Approximately 5–7 g of each mineral was then added to a gold cylinder ($1/2'' \times 5''$) that was placed inside the reactor. The walls of the gold cylinder were perforated with numerous $1/16''$ holes to allow experimental fluid to reach the minerals and both ends were crimped after adding the minerals. Use of the gold cylinder facilitated the removal of the minerals at the end of the experiment; it was not meant to act as a $H_{2(aq)}$ membrane. In addition to hematite and magnetite, K-feldspar, muscovite, and quartz were also present in the experiment to serve as a pH buffer. KCl-H_2O fluids were therefore used instead of NaCl-H_2O to maintain consistency between the composition of the fluid and minerals and avoid reactions involving Na-K solid solutions.

After inserting the gold cylinder into the reactor, the main nut was sealed and ultra-pure argon was flushed through the reactor for at least 20 min to expel room air. The reactor was then connected to an ISCO syringe pump and experimental fluid was pumped into the bottom of the reactor, while the remaining argon was allowed to escape through the vapor sampling valve (see Scheuermann et al., 2018). All valves were closed once the reactor was filled with solution and it was then brought to the experimental pressure and temperature. Before introducing the experimental solution into the reactor, it was put under vacuum and sonicated for 30 minutes to purge dissolved gases. Additionally, 200 μmol/kg formic acid (CH_2O_2) was added to the experimental solution. Formic acid decomposes into H_2 and CO_2 above 250 °C (McCollom and Seewald, 2003; Pester et al., 2015) and was included to ensure that any residual dissolved O_2 did not adversely affect the mineral redox buffer.

The experimental design used here allows for multiple samples of both vapors and single-phase fluids to be taken at various temperatures without the need to return to ambient conditions between samples. Once at the appropriate pressure and temperature, the entire system was allowed to react for a minimum of 4 days at 400 and 425 °C, 3 days at 450 and 2 days at 500 °C to achieve equilibrium, consistent with previously determined time constraints on silicate-fluid and Fe-oxide- fluid equilibrium at similar temperatures (Kishima and Sakai, 1984a; Foustoukos and Seyfried, 2007). These reaction times were also confirmed by reversing equilibrium through temperature adjustment and measuring fluid chemistry. The autoclave was positioned at a slight angle above horizontal. This orientation promoted segregation of vapor and liquid, and minimized temperature gradients along the length of the reactor. It is important to note that the hematite-magnetite assemblage fixes $f\,H_2$ within the entire system at a unique value at a given temperature. Thus, the minerals need not contact both fluid phases in order to effectively buffer $f\,H_2$.

Prior to sampling, approximately 0.3 g of fluid were removed to flush the capillary line. Aliquots for cations were diluted at least 4-fold with 1 M Optima HCl to prevent precipitation of iron bearing phases. The aliquot for $H_{2(aq)}$ analysis was collected in a gas tight syringe, diluted with ultra-pure N_2 and immediately analyzed. Additional aliquots were also taken to determine the concentrations of dissolved anions and $pH_{25°C}$.

2.3. Analytical methods

All cations, dissolved silica, and minerals (following hydrofluoric acid digestion, see below) were measured by inductively coupled plasma optical emission spectroscopy (ICP-OES). Cl was measured by ion chromatography (IC). Samples measured by ICP-OES were analyzed three times and those measured by IC were run twice. The average of these values is reported. Uncertainties for the ICP-OES and IC are 3 % and 2 %, respectively (2σ, Table 1). The concentration of $H_{2(aq)}$ in all samples was measured using an Agilent 6980 gas chromatograph (GC), equipped with a carbon molecular sieve column (Carboxen™ 1010 PLOT) and thermal conductivity detector. Prior to each sample, the GC was calibrated with a gas standard containing 1% H_2 gas. Reproducibility of the 1% standard was always within 10% and all $H_{2(aq)}$ concentrations were calculated using an averaged ($n = 10$) 1% standard. $pH_{25°C}$ was measured using a Thermo-Ross electrode that was calibrated with pH 4, 7, and 10 buffers before each measurement.

Prior to ICP-OES analysis, minerals were acid digested. The sample was powdered and 0.1 g was added to a 10 mL mixture of HF, HNO_3, and deionized water. The powder and acid mixture were loaded into a sealed Teflon cylinder and were allowed to digest for 2 hours at 200 °C. Standard rock samples (BHVO-1 and G-2) provided by the United States Geological Survey were digested and analyzed concurrently with the experimental samples in order to verify results. The USGS standards returned within ±10% of the stated values of the major oxides.

The minerals were also analyzed by x-ray powder diffraction (XRD). A Rigaku Miniflex© X-ray diffractometer with cobalt radiation was used. 2Θ angles were then

Table 1
Chemical composition of experimental samples and calculated $Y_{H_2\text{-}Cl}$ values.

Temp. (°C)	Pressure (bar)	Phase	Rxn time (days)	pH $_{25}$ °C	H_2 (μmol/kg)	K (mmol/kg)	Cl (mmol/kg)	Density (g/cm^3)	$Y_{H_2\text{-}Cl}$ (bar/molal)
400	215	vap	10	3.86	1222	11	13	0.12	9
400	240	vap	7	3.53	545	15	16	0.15	21
400	260	vap	4	3.60	372	26	27	0.19	32
400	280	SP	4	4.10	145	674	659	0.51	84
400	330	SP	13	4.2	40	931	1012	0.61	316
425	322	vap	7	3.26	294	80	79	0.24	47
425	335	vap	5	2.39	219	383	390	0.30	64
425	338	vap	4	3.58	236	618	602	0.41	60
450	350	vap	6	3.55	890	43	45	0.21	17
450	380	vap	5	3.06	519	93	96	0.25	30
450	400	vap	5	3.09	346	187	183	0.30	47
450	415	vap	7	3.63	300	529	535	0.38	55
450	430	SP	3	3.09	131	800	827	0.46	128
450	470	SP	4	3.43	127	790	819	0.50	137
500	400	vap	5	3.03	4237	31	33	0.18	4
500	430	vap	3	3.03	2210	49	52	0.20	8
500	470	vap	4	3	1650	83	87	0.24	12
500	510	vap	2	2.95	1206	173	182	0.28	17

SP = single-phase fluid.

converted to the Cu Kα scale. The specific range of values over which the measurements were made are provided in the figures found in the Appendix A.

2.4. Calculation of Y_{H_2}

In order for $H_{2(aq)}$ to become a more quantitative tool in understanding mass-transfer processes in axial hydrothermal systems, the fugacity-concentration relationship must be known to correlate measured concentrations to thermodynamic predictions of $f\,H_2$. While the $f\,H_2$-concentration relationship has been determined in pure water at temperature–pressure conditions relevant to MOR systems (Kishima and Sakai, 1984a), the effect of dissolved salt can cause $H_{2(aq)}$ concentrations to differ significantly from those measured in pure water (Drummond, 1981). Here, Y_{H_2} denotes the fugacity-concentration relationship in the pure water system and $Y_{H_2\text{-}Cl}$ indicates a saline bearing aqueous fluid.

In this study, hematite and magnetite were used to buffer $f\,O_2$ through the following reaction

$$\text{Hematite} = \tfrac{1}{2}\,O_{2(g)} + 2\,\text{Magnetite} \quad (3)$$

The conversion to $f\,H_2$ requires combination of Eq. (3) with Eq. (4)

$$H_{2(g)} + \tfrac{1}{2}\,O_{2(g)} = H_2O_{(l)} \quad (4)$$

to yield (Kishima and Sakai, 1984a)

$$\text{Hematite} + H_{2(g)} = 2\,\text{Magnetite} + H_2O_{(l)} \quad (5)$$

$f\,H_2$ can then be calculated, assuming pure mineral phases, as follows:

$$fH_2 = K_5^{-1} \quad (6)$$

where K_5 represents the equilibrium constant for Eq. (5). Y_{H_2} and $Y_{H_2\text{-}Cl}$ (bar/molal) are then determined as the ratio of $f\,H_2$ to measured concentration in the aqueous fluid

$$Y_{H_2} = fH_2/[H_{2(aq)}] \quad (7)$$

Y_{H_2} can be converted to the well-known Henry's law constant, k_H (bar),

$$k_H = N_w Y \quad (8)$$

where $N_w = 55.51$ mol kg^{-1} H_2O (Akinfiev and Diamond, 2003).

The relevant thermodynamic data for calculation of $f\,H_2$ are taken from SUPCRT92 (Johnson et al., 1992). SUPCRT92 utilizes the revised Helgeson-Kirkham-Flowers equation of state to calculate the thermodynamic properties of gases, aqueous solutes and water (Tanger and Helgeson, 1988; Shock and Helgeson, 1988; Shock et al., 1989; Shock and Helgeson, 1990). The standard state for gases is the ideal gas at the temperature of interest and 1 bar. The standard state for minerals and water is the pure substance at the pressure and temperature of interest. Aqueous solutes are treated as ideal in a hypothetical one molal solution referenced to infinite dilution.

log $f\,H_2$ values generated by SUPCRT92 for the mineral buffers hematite-magnetite and pyrite-pyrrhotite-magnetite are all within 0.5 log units or less of those determined experimentally by Kishima and Sakai (1984a,b) and Kishima (1989) in the temperature range 400–500 °C. The log $f\,H_2$ data given by SUPCRT92 are always greater than those given by Kishima and Sakai (1984a,b) and Kishima (1989). There is similar agreement between $f\,H_2$ as calculated by SUPCRT92 and the experimental data of Chou (1978) between 600–800 °C. Variations in calculated log $f\,H_2$ stem from differences in the thermodynamic properties of the mineral phases and water, since $H_{2(g)}$ is the reference state for hydrogen and therefore does not contribute to the free energy budget of reaction (5) (e.g, Anderson and Crerar, 1993). In a series of more recent publications, Holland and Powell (1998, 2011) present a database of internally consistent thermodynamic data for mineral phases based on an extensive number of experimental

measurements. Comparison of log f H_2 as given by SUPCRT92 and the data of Holland and Powell (2011) yields results within 0.02 and 0.1 log units for hematite-magnetite and pyrite-pyrrhotite-magnetite, respectively.

The good agreement with the data of Kishima and Sakai (1984a,b), Kishima (1989) and Chou (1978) and the excellent agreement with Holland and Powell (2011) warrants the use of SUPCRT92 to calculate Y_{H_2}, as outlined above. All Y_{H_2} and $Y_{H_2\text{-}Cl}$ values presented in this contribution, regardless of the source of experimental $H_{2(aq)}$ measurements, have been calculated using f H_2 as defined by data in SUPCRT92 for the appropriate mineral assemblage.

The use of f H_2 in this study stems from the well-documented uncertainty of HKF predictions of the thermodynamic properties of neutral aqueous species, including $H_{2(aq)}$ and $H_2S_{(aq)}$, above the critical point of pure water (Plyasunov et al., 2000; Akinfiev and Diamond, 2003). For example, at 275 bar, the difference between experimentally determined and theoretically calculated equilibrium constants for Eq. (9), K_9, is 1.3 log units at 400 °C and 2.4 log units at 450 °C (Eklund et al., 1997).

$$f H_{2(g)} = a H_{2(aq)} \quad (9)$$

While more recent equations have improved the accuracy of K_9 (e.g., Plyasunov et al., 2000; Akinfiev and Diamond, 2003), these equations are not yet integrated into software codes that facilitate calculation of fluid-mineral equilibria.

2.5. Calculating fluid density

In this study, fluid density is calculated using the equations of Driesner (2007), modified to incorporate the difference in molecular weight between NaCl and KCl. Modification of the correlation of Driesner (2007) yields agreement within 10% of experimental measurements of KCl-H_2O density at hydrothermal conditions, 300–700 °C, 800–2000 bar (Khaibullin and Borisov, 1966; Bodnar and Sterner, 1985).

3. RESULTS

Fluid samples were collected at pressure–temperature conditions that yield a wide range of KCl concentration (12–1000 mmol/kg) and fluid density (0.1–0.5 g cm^{-3}, Table 1). Four single-phase fluids and fourteen low-density vapors were collected. Comparison of experimental KCl concentrations (the average of measured K^+ and Cl^-) of vapors with the numerical model of Driesner and Heinrich (2007) shows very good agreement (Fig. 1) and indicates that the fluid matrix attained equilibrium between coexisting vapor and liquid. While the model of Driesner and Heinrich (2007) is based on experiments in the NaCl-H_2O system, the similar chemical properties of K^+ and Na^+ yield compositions of coexisting vapor–liquid that are indistinguishable within experimental error (Liebscher, 2007). Within the vapor–liquid region of the KCl-H_2O system, the composition of the vapor and liquid are fixed at a given pressure–temperature condition and do not depend on the KCl composition of the fluid prior to phase separation (Liebscher, 2007). The mass ratio of vapor to liquid changes as a function of bulk KCl content, but this ratio does not affect the solubility of dissolved components such as $H_{2(aq)}$.

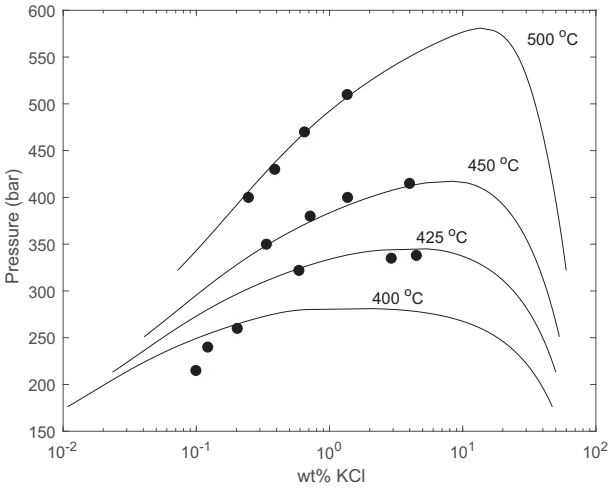

Fig. 1. Measured KCl concentrations in the low-salinity vapors plotted against the model isotherms of Driesner and Heinrich (2007). There is good agreement between measured and predicted concentrations highlighting the accuracy of the pressure–temperature control system. Samples of high-salinity liquids were not collected as part of this study.

$H_{2(aq)}$ concentrations display a clear dependence on pressure, Cl concentration, and temperature (Fig. 2). Along an isotherm, $H_{2(aq)}$ concentration decreases with increasing pressure and Cl concentration (Table 1). This pattern is shown in Fig. 2 as a function of density in order to more easily compare data along the four different isotherms. As

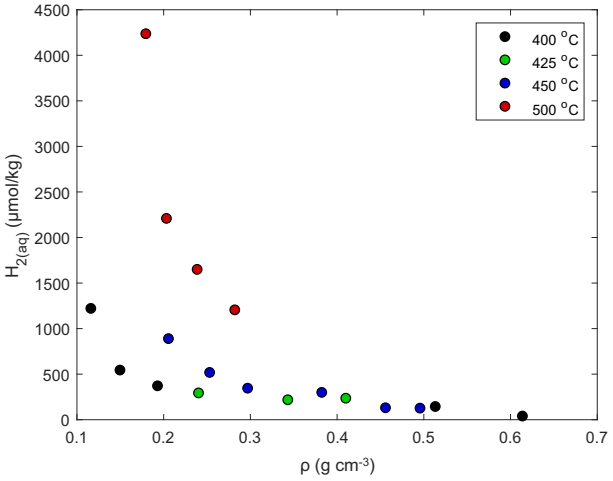

Fig. 2. Measured $H_{2(aq)}$ concentrations plotted as a function of density along the four different isotherms investigated in this study. Density is used in lieu of pressure in order to display the results on an overlapping scale. Samples with density greater or equal to 0.45 g cm^{-3} represent single-phase fluids. The vapor samples have density less than 0.45 g cm^{-3}.

pressure and/or Cl concentration increase, density increases along the isotherms. The data also indicate increasing $H_{2(aq)}$ concentration as temperature increases at constant density. For a given pressure–temperature condition, a range of $\pm$ 40 μmol/kg $H_{2(aq)}$ was determined by multiple measurements, each taken after temperature excursions. Bulk mineral chemistry (Table A1) and XRD analysis (Fig. A1) indicates that the hematite and magnetite crystals did not change composition over the course of the experiment.

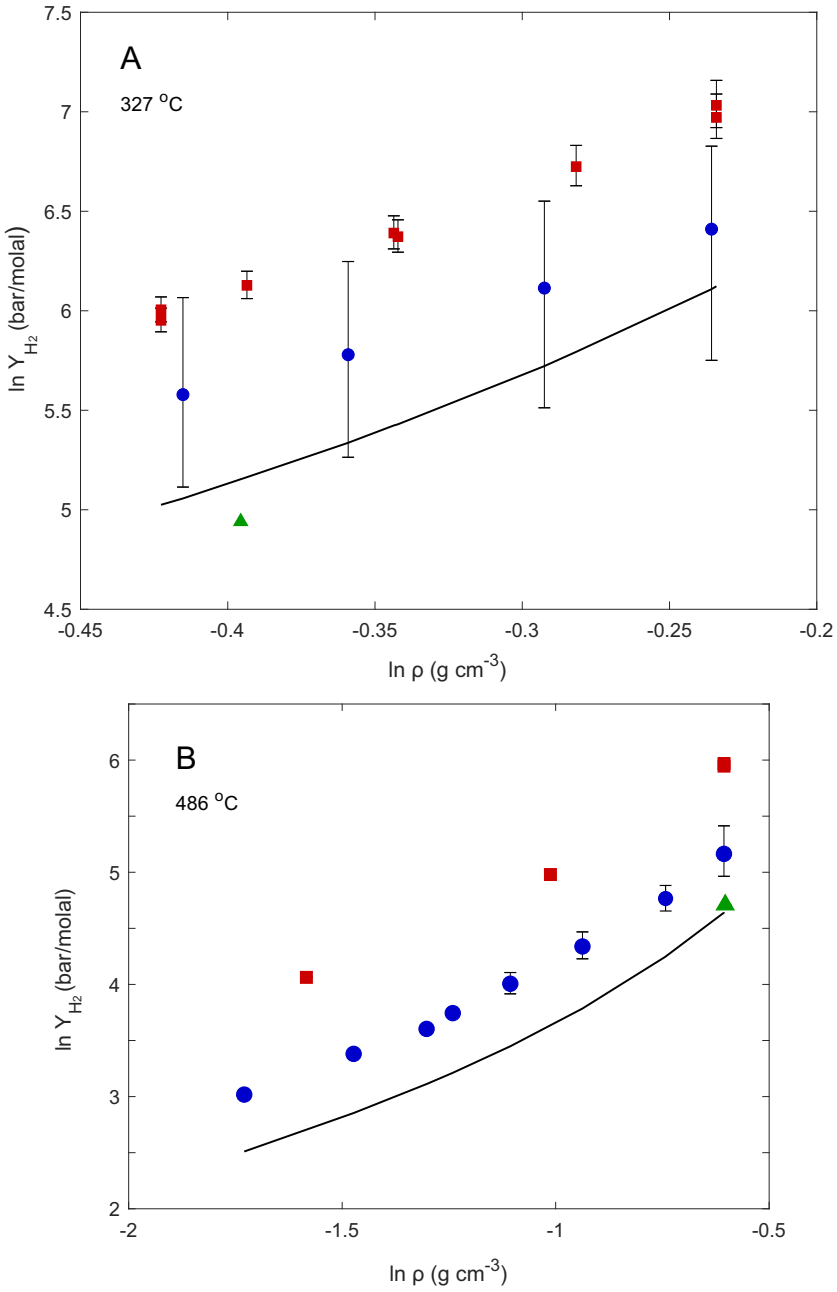

Fig. 3. The natural logarithm of Y_{H_2} (bar/molal) as a function of the natural logarithm of fluid density in the pure water system at (A) 327 °C, 140–1000 bar and (B) 486 °C, 380–1000 bar. Along an isotherm, ln Y_{H_2} is an approximately linear function of ln ρ. Experimental $H_{2(aq)}$ concentrations are from Kishima and Sakai (1984a,b) and Kishima (1989), but Y_{H_2} have been calculated using $f\,H_2$ from SUPCRT92. The three symbols represent different experiments, red: pyrite-pyrrhotite-magnetite, blue: hematite-magnetite, and green: nickel-nickel oxide. The solid lines represent predictions of the Akinfiev and Diamond (2003) equation of state. Error bars are estimated based on the differences between $H_{2(aq)}$ concentrations for multiple samples collected at the same PT condition (Kishima, 1989). In (B), data from Kishima (1989) PPM experiments are from 490 °C.

4. DISCUSSION

4.1. Comparison with previous $H_{2(aq)}$ solubility measurements

The experiments of Kishima and Sakai (1984a,b) and Kishima (1989) provide the most extensive measurements of $H_{2(aq)}$ solubility in mineral buffered fluids at elevated pressures and temperatures. All experiments were performed in the pure water system between 296–500 °C, 100–1000 bar in gold cell hydrothermal reactors (Seyfried et al., 1987). Kishima and Sakai (1984a,b) measured $H_{2(aq)}$ as buffered by hematite-magnetite (HM) and nickel-nickel oxide (NNO), while Kishima (1989) measured $H_{2(aq)}$ solubility as dictated by pyrite-pyrrhotite-magnetite (PPM).

The experiments of Kishima and Sakai (1984a,b) and Kishima (1989) indicate that along an isotherm, Y_{H_2} increases with increasing pressure, while along isobars, Y_{H_2} decreases as temperature increases. In other words, Y_{H_2} decreases in magnitude as density decreases and the fluid becomes more gas-like. At 416 °C, for example, Y_{H_2} increases from 64 to 335 bar/molal as pressure increases from 365 to 1000 bar. Y_{H_2} decreases from 785 to 175 bar/molal as temperature increases from 300 to 490 °C at 1000 bar. The behavior of Y_{H_2} as a function of pressure and temperature is decidedly non-linear (Kishima and Sakai, 1984a; Kishima, 1989), but can be simplified considerably by converting pressure to density (ρ). ln Y_{H_2} is then an approximately linear function of ln ρ along an isotherm (Fig. 3).

A linear relationship between gas solubility and fluid density has been previously recognized based on observations of experimental data at temperatures below the critical point of pure water (Japas and Sengers, 1989, and references therein). In fact, Akinfiev and Diamond (2003) derived an equation of state (EoS) for aqueous nonelectrolytes that relies on the relationship between gas solubility and fluid density in order to regress the values for several empirical fit parameters. The empirical parameters relevant to $H_{2(aq)}$ are based on experimental data collected from 0 to 486 °C, 1 to 1000 bar in the pure water system (i.e., infinite dilution), including the data of Kishima and Sakai (1984a). The Akinfiev and Diamond (2003) EoS is compatible with the Helgeson-Kirkham-Flowers EoS and therefore the results can be compared with Y_{H_2} as generated from experimental data (see Eq. (8) for conversion). There is generally good agreement between the EoS predictions and the diverse dataset of experiments along the vapor saturation curve (see Fig. 1b in Akinfiev and Diamond, 2003). However, at pressures above saturation the disagreement between experimental data and EoS predictions increases. At 327 °C and 486 °C (Fig. 3), the Akinfiev and Diamond (2003) EoS predicts ln Y_{H_2} values that are approximately 0.5 natural log units lower than that given by the hematite-magnetite experiments of Kishima and Sakai (1984a). Depending on the value of ln Y_{H_2} a difference of 0.5 natural log units can lead to deviations between calculated and measured Y_{H_2} of up to 155 bar/molal. Given the discrepancy between the hematite-magnetite experimental data and the Akinfiev and Diamond (2003) EoS, the hematite-magnetite data have been fit to an empirical function of temperature and fluid density in order to facilitate comparison with the experimental data collected in salt-bearing fluids (this study, Ding and Seyfried, 1990). The empirical equation is as follows:

$$\ln Y_{H_2-KS} = 7.983 - 0.001818T + 6.341\ln\rho - 0.005568T\ln\rho + 0.7477\ln\rho^2 \quad (10)$$

Temperature is given in °C and density in g cm^{-3}. Fig. A2 provides a comparison of measured and calculated Y_{H_2} values using Eq. (10).

The larger disagreement between the predictions of the Akinfiev and Diamond (2003) EoS and the PPM experiments of Kishima (1989, Fig. 3), may be the result of solid solution in pyrrhotite (Barton and Skinner, 1979), which lowers the activity of FeS. A lower FeS activity will cause Y_{H_2} to be less than that calculated assuming a pure mineral. Unfortunately, Kishima (1989) does not report the composition of pyrrhotite used in the experiments. However,

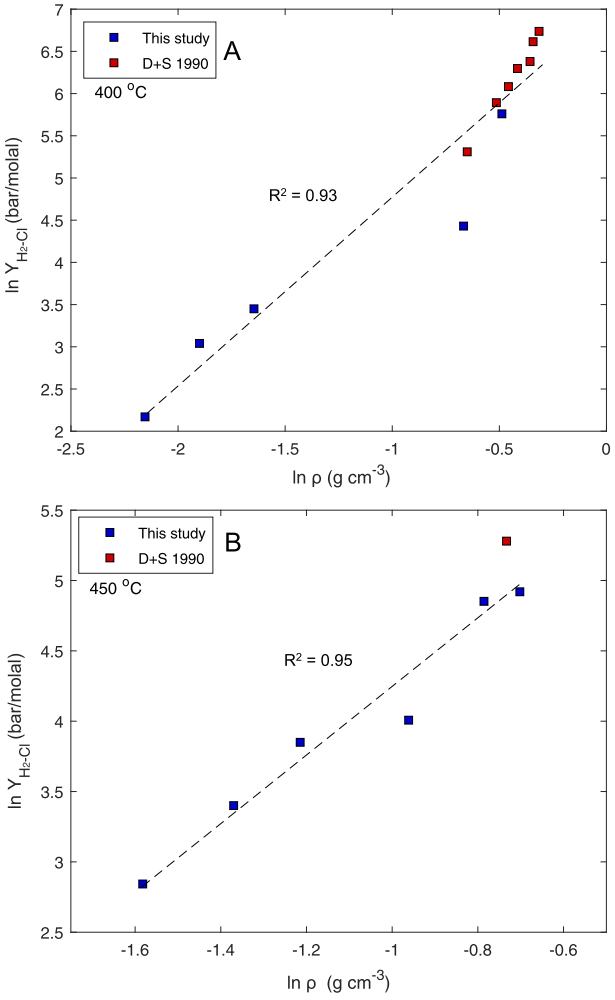

Fig. 4. ln Y_{H_2-Cl} as calculated in the NaCl-H_2O (Ding and Seyfried, 1990) and KCl-H_2O (this study) at 400 °C (A) and 450 °C (B). ln Y_{H_2-Cl} is a linear function of ln ρ along an isotherm, regardless of whether samples are low-density vapors or single-phase fluids. Dashed lines represent linear regressions of the data.

calculations indicate that a minimal decrease in pyrrhotite activity, $Po_{0.8\text{-}0.9}$, causes Y_{H_2} to decrease and show good agreement with Y_{H_2} as calculated from the HM and NNO experiments (Kishima and Sakai, 1984a,b).

The addition of significant quantities of dissolved salts (e.g., NaCl or KCl) complicates the prediction of $H_{2(aq)}$ solubility in natural geothermal fluids. As the concentration of dissolved salt increases in an aqueous fluid at constant temperature and pressure $H_{2(aq)}$ solubility decreases. The phenomena of decreasing $H_{2(aq)}$ solubility with increasing salt concentration has been deemed 'salting-out' and is a well-documented process that affects the solubility of all neutral aqueous species (e.g., Oelkers and Helgeson, 1991; Sharygin et al., 2002). In the context of the current study, decreased $H_{2(aq)}$ solubility in saline fluids will cause $Y_{H_2\text{-}Cl}$ to be larger than Y_{H_2} since $f\,H_2$ remains constant at a given pressure–temperature condition, regardless of fluid composition (Eq. (7)). The presence of salt does not change the behavior of $Y_{H_2\text{-}Cl}$ as a function of pressure and temperature as compared to Y_{H_2}. Values of $Y_{H_2\text{-}Cl}$ decrease as the fluid density decreases (Fig. 4).

In addition to the results of the current study, the experiments of Ding and Seyfried (1990) provide data for $H_{2(aq)}$ solubility in salt-bearing aqueous fluids at conditions relevant to MOR vent systems. These experiments utilized the PPM mineral assemblage to buffer $H_{2(aq)}$ between 300–450 °C, 300–500 bar, and 560–2000 mmol/kg NaCl (Table 2, Appendix A). $Y_{H_2\text{-}Cl}$ as calculated from the new experimental data and those of Ding and Seyfried (1990) show a similar trend to Y_{H_2} (Kishima and Sakai, 1984a,b; Kishima, 1989) when plotted as a function of density and temperature (Fig. 4). As expected, $Y_{H_2\text{-}Cl}$ calculated from both sets of experiments are larger than those in the pure water system (Fig. 5). At 350 °C, $Y_{H_2\text{-}Cl}$ as calculated from the PPM experiments (Ding and Seyfried, 1990) are approximately two to three times larger than those predicted for the pure water system by the Akinfiev and Diamond (2003) EoS or the data of Kishima and Sakai (1984a,b, Fig. 5a). This offset between $Y_{H_2\text{-}Cl}$ and Y_{H_2} is essentially constant because the experimental NaCl concentration remains within a narrow range, 560–600 mmol/kg. At 400–450 °C, the offset between $Y_{H_2\text{-}Cl}$ and Y_{H_2} changes (Fig. 5b-d) because the KCl concentration in the current study varies between 15–1000 mmol/kg, and NaCl varies between 500–2000 mmol/kg in the study of Ding and Seyfried (1990). At 400 °C, 215 bar, the KCl concentration in the low-density vapor is 13 mmol/kg and $Y_{H_2\text{-}Cl}$ calculated at this condition, 9, is within error of Y_{H_2}, 6. In contrast, $Y_{H_2\text{-}Cl}$ is 192 at 450 °C, 500 bar, 570 mmol/kg NaCl, while $Y_{H_2} = 45$ at the same pressure and temperature. The difference between $Y_{H_2\text{-}Cl}$ and Y_{H_2} further increases as dissolved NaCl concentrations reach 1–2 molal (Fig. 5b).

Data at 500 °C, collected as part of the current study, deviate from the pattern seen at lower temperature. $Y_{H_2\text{-}Cl}$ at 500 °C are 1.3–3 times lower than values predicted for the pure water system (Fig. 5e). It is possible that the Akinfiev and Diamond (2003) EoS and Kishima and Sakai (1984a,b) data overestimate Y_{H_2} at 500 °C, since these datasets have an upper bound of 486 °C. Alternatively, the relatively small differences between Y_{H_2} and $Y_{H_2\text{-}Cl}$ and the low Cl concentration of the experimental samples (33–182 mmol/kg Cl) suggests that at such high temperatures Y_{H_2} and $Y_{H_2\text{-}Cl}$ may converge to similar values. We therefore posit that the pattern seen in Fig. 5e, $Y_{H_2\text{-}Cl} < Y_{H_2}$, is the result of inconsistency between datasets and does not indicate 'salting-in' behavior.

Table 2
Experimental data from Ding and Seyfried (1990).

Temperature (°C)	Pressure (bar)	Cl (mmol/kg)	H_2 (mmol/kg)	H_2S (mmol/kg)	Density (g cm^{-3})	$Y_{H_2\text{-}Cl}$ (bar/molal)	$Y_{H_2S\text{-}Cl}$ (bar/molal)
300	500	576	0.21	1.92	0.81	1073	84
300	400	598	0.23	2.04	0.80	945	74
300	300	572	0.25	2.25	0.78	843	64
350	500	567	0.37	5.96	0.73	711	77
350	400	589	0.41	6.79	0.71	599	64
350	300	581	0.48	7.1	0.69	488	58
375	500	594	0.46	10.78	0.69	591	67
375	400	578	0.54	11.69	0.66	479	58
375	300	587	0.70	12	0.63	350	53
400	500	594	0.64	18.75	0.63	438	50
400	400	632	0.73	19.82	0.60	362	51
400	300	592	1.23	26.03	0.52	202	42
400	500	1454	0.47	13.8	0.70	590	68
400	500	1951	0.33	11.16	0.73	843	84
400	400	1316	0.49	15.73	0.66	543	64
400	400	2012	0.35	13.15	0.71	746	77
425	500	570	0.97	31.1	0.56	293	50
425	400	556	1.40	38.9	0.49	190	37
450	500	572	1.46	54.99	0.48	195	39

Na concentrations are, within error, equal to Cl.
The experiments of Ding and Seyfried (1990) were performed in flexible gold cell hydrothermal reactors (Seyfried et al., 1987).
All samples are single-phase fluids.

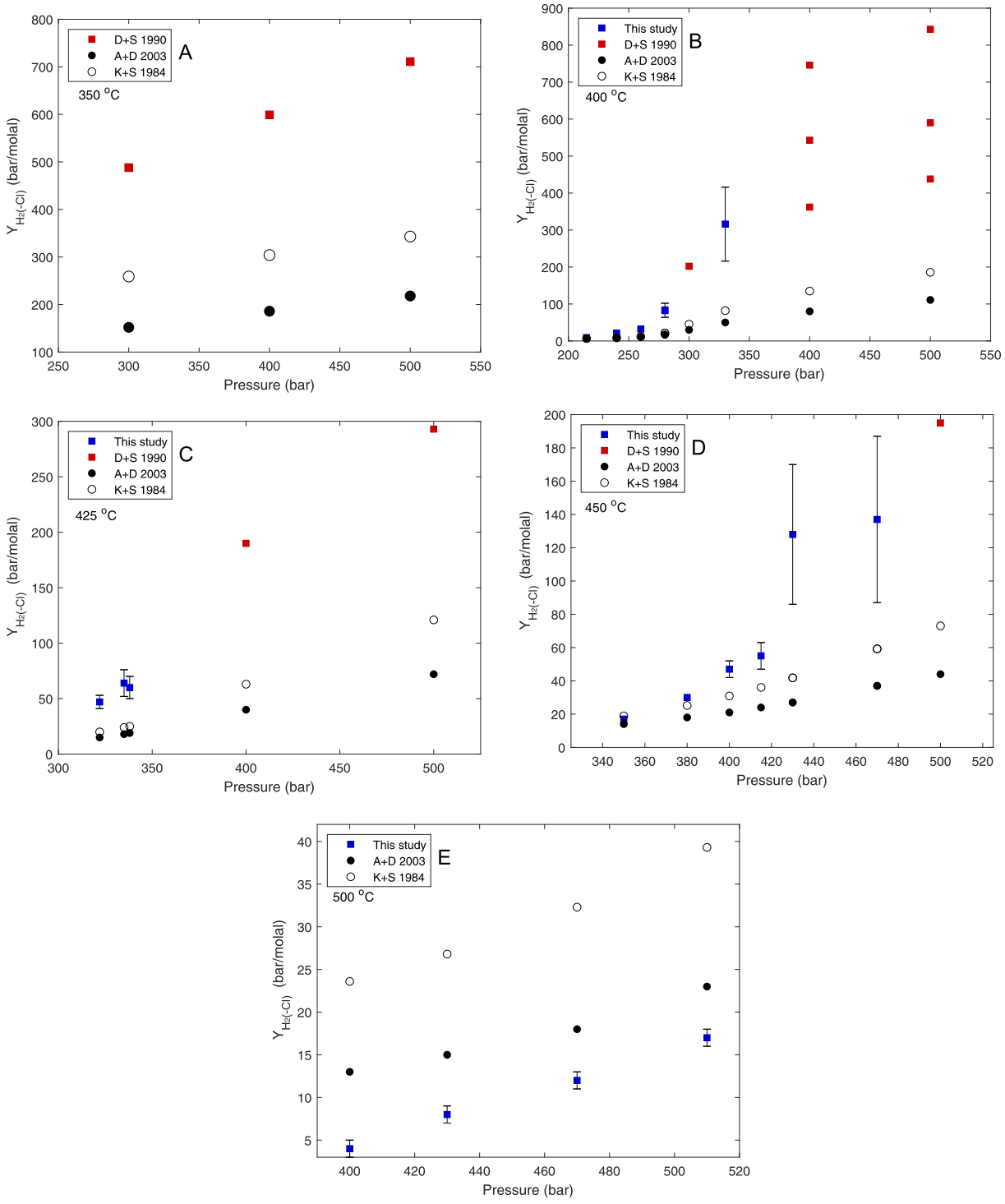

Fig. 5. Comparison of $Y_{H_2\text{-}Cl}$ with Y_{H_2} as a function of pressure along various isotherms. Y_{H_2} in the pure water system come from the Akinfiev and Diamond (2003) EoS (filled circles) or the experiments of Kishima and Sakai (1984a,b, empty circles). The data of Kishima and Sakai (1984a,b) were extrapolated using Eq. (10). The red squares represent the data of Ding and Seyfried (1990) and the blue squares are from this study. NaCl or KCl concentrations can be found in Tables 1 and 2. Error bars for data from this study are calculated based on experimental uncertainty, ±40 μmol/kg $H_{2(aq)}$. Larger error bars correspond to samples with lower $H_{2(aq)}$ concentrations and thus larger values of $Y_{H_2\text{-}Cl}$.

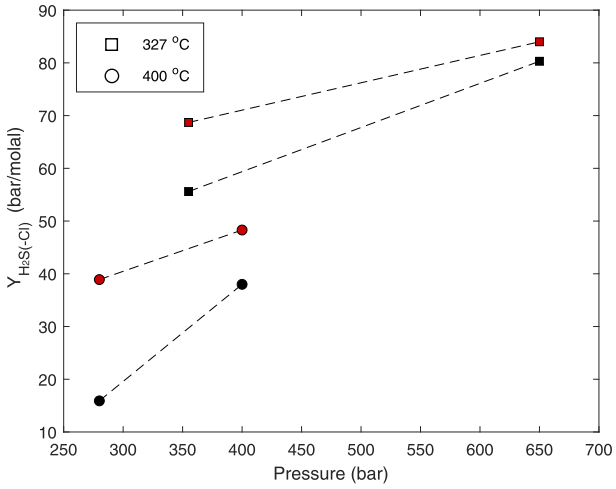

Fig. 6. $Y_{H_2S\text{-}Cl}$ as calculated in the NaCl-H_2O system (Ding and Seyfried, 1990, red symbols) compared with the data of Kishima (1989, black symbols) in the pure water system. The shape of the symbols indicates the temperature as given in the legend. Tie lines are to guide the eye.

ln $Y_{H_2\text{-}Cl}$ as calculated from the salt-bearing experiments (this study, Ding and Seyfried, 1990), were fit to the following empirical equation of temperature (°C) and density (g cm^{-3})

$$\ln Y_{H_2-Cl} = 7.651 - 0.001214T + 0.0626\ln\rho + 0.00736T\ln\rho + 0.3876(\ln\rho)^2 \quad (11)$$

Eq. (11) is based on experimental data collected from single-phase fluids and low-density vapors between 300–500 °C, 210–510 bar and 0–2000 mmol/kg dissolved NaCl (or KCl). While data for samples containing greater than 1000 mmol/kg NaCl were included in the regression of equation (11), $Y_{H_2\text{-}Cl}$ calculated for these high salinity samples deviate from measured values more strongly than those calculated for less saline fluids (Fig. A3). The incorporation of both single-phase and low-density vapors in the regression of equation (11) is based on the growing recognition that phase separation does not represent a discontinuity in the description of solubility (Scheuermann et al. 2018, 2019). This can be seen in the H_2 solubility data as ln $Y_{H_2\text{-}Cl}$ is a linear function of ln ρ for samples taken along the 400 and 450 °C isotherms (Fig. 4).

4.2. Previous measurements of $H_2S_{(aq)}$ solubility and calculation of $Y_{H_2S\text{-}Cl}$

Measurements of $H_2S_{(aq)}$ solubility at conditions relevant to this work have been made by Kishima (1989) in the pure water system (300–500 °C, 100–1000 bar) and Ding and Seyfried (1990) in the NaCl-H_2O system (300–450 °C, 300–500 bar, 560–2000 mmol/kg NaCl). Both Ding and Seyfried (1990) and Kishima (1989) used the pyrite-pyrrhotite-magnetite assemblage to buffer $H_2S_{(g)}$:

$$2\,\text{Pyrrhotite} + \text{Pyrite} + 4\,H_2O = 4\,H_2S_{(g)} + \text{Magnetite} \quad (12)$$

Y_{H_2S} and $Y_{H_2\text{-}Cl}$ can be calculated using a modified version of equation (7). Requisite thermodynamic data for calculating f H_2S, assuming pure minerals, are taken from SUPCRT92.

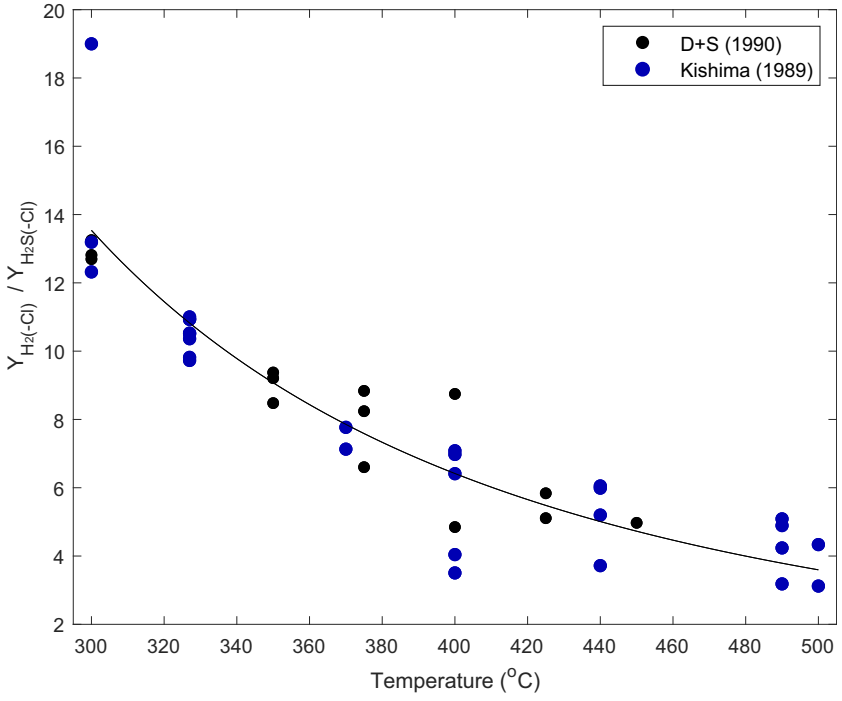

Fig. 7. Y_{H_2}/Y_{H_2S} (blue circles) and $Y_{H_2\text{-}Cl}/Y_{H_2S\text{-}Cl}$ (black circles) calculated using the experimental data of Kishima (1989) and Ding and Seyfried (1990). At constant temperature, the range of values is a function of pressure. The black line is an empirical fit to the data, $Y_{H_2}/Y_{H_2S} = 3.63 \times 10^7\ T^{-2.595}$.

Similar to $Y_{H_2\text{-Cl}}$, $Y_{H_2S\text{-Cl}}$ is an approximately linear function of fluid density at constant temperature (Fig. A4). The data of Ding and Seyfried (1990) were therefore used to regress the following equation for $Y_{H_2S\text{-Cl}}$:

$$\ln Y_{H_2S-Cl} = 2.512 + 0.009898T + 2.462\ln\rho + 0.01325T\ln\rho + 5.36(\ln\rho)^2 \quad (13)$$

Eq. (13) is based on experimental measurements between 300–450 °C, 300–500 bar and 550–2000 mmol/kg NaCl (Table 2), conditions entirely within the single-phase field. Similar to Eq. (11), Eq. (13) reproduces $Y_{H_2S\text{-Cl}}$ values most accurately for fluids with NaCl content less than 1000 mmol/kg (Fig. A5).

$Y_{H_2S\text{-Cl}}$ displays similar behavior to $Y_{H_2\text{-Cl}}$ in that values of $Y_{H_2S\text{-Cl}}$ decrease with decreasing fluid density and $Y_{H_2S\text{-Cl}}$ is larger than Y_{H_2S} owing to salting-out effects (Fig. 6). The magnitude of $Y_{H2S\text{-Cl}}$, however, is smaller than that of $Y_{H_2\text{-Cl}}$. $Y_{H_2S\text{-Cl}}$ reaches a maximum of 84 bar/molal at 300 °C, 550 mmol/kg NaCl, while at the same temperature and salt concentration the maximum value of $Y_{H_2\text{-Cl}}$ is 1072 bar/molal. These differences between values of $Y_{H_2S\text{-Cl}}$ and $Y_{H_2\text{-Cl}}$ are consistent with previous data that demonstrate increased solubility of $H_2S_{(aq)}$ as compared to $H_{2(aq)}$, at constant temperature, pressure and salt concentration (Drummond, 1981). As temperature increases above 300 °C the difference between $Y_{H_2\text{-Cl}}$ and $Y_{H_2S\text{-Cl}}$ decreases (Fig. 7). The decrease in Y_{H_2}/Y_{H_2S} is greatest at lower temperatures and decreases with increasing temperature. The presence of salt does not significantly alter $Y_{H_2\text{-Cl}}/Y_{H_2S\text{-Cl}}$, as compared to Y_{H_2}/Y_{H_2S} at the same temperature and pressure. For example, at 300 °C, 500 bar (500 mmol/kg NaCl) and 400 °C, 400 bar (500 mmol/kg NaCl), $Y_{H_2\text{-Cl}}/Y_{H_2S\text{-Cl}}$ is 12.9 and 3.9, respectively. At the same pressures and temperatures in the pure water system Y_{H_2}/Y_{H2S} is 12.3 and 4.1. The presence of NaCl (or KCl) appears to cause both $H_{2(aq)}$ and $H_2S_{(aq)}$ to 'salt-out' equally and therefore the $Y_{H_2\text{-Cl}}/Y_{H_2S\text{-Cl}}$ ratio is equal to its counterpart in the pure water system. Further study will be necessary to provide a more thorough explanation for the observation that salt does not appear to change the $Y_{H_2\text{-Cl}}/Y_{H_2S\text{-Cl}}$ ratio as compared to Y_{H_2}/Y_{H_2S}.

The importance of accurately quantifying $Y_{H_2S\text{-Cl}}$ and $Y_{H_2\text{-Cl}}$ can be seen by calculating the $H_2S_{(aq)}$ and $H_{2(aq)}$ concentrations in equilibrium with a given mineral assemblage at hydrothermal conditions (Fig. 8), with and without explicit consideration of $Y_{H_2S\text{-Cl}}$ and $Y_{H_2\text{-Cl}}$ data. When dissolved gas concentrations are calculated using the assumption that concentration is equal to the thermodynamic activity, as calculated by the HKF EoS, calculations show substantial overestimation of the equilibrium concentration.

4.3. Dissolved gases as a constraint on hydrothermal alteration at the Piccard vent field

At 4957–4987 m depth, the Piccard vent field (also known as the Beebe vent field) on the Mid-Cayman Rise is the deepest known hydrothermal system on earth (Connelly et al., 2012). The extreme depth notwithstanding, the Cl concentration of end member fluids, 350 mmol/kg, is less than that of seawater, indicating phase separation occurs in the subsurface (McDermott et al., 2018). A minimum temperature limit of 483 °C can be calculated assuming phase separation occurs at the seafloor pressure of approximately 500 bar. This is a minimum temperature because in the rare cases where phase separation occurs near the seafloor both vapor and conjugate liquid actively vent to the seafloor (Von Damm et al., 2003). Only the vapor has been observed at Piccard and thus phase separation more likely occurs at depth within the oceanic crust. Application of the recently calibrated Si-Cl geothermobarometer indicates phase separation occurs at 540

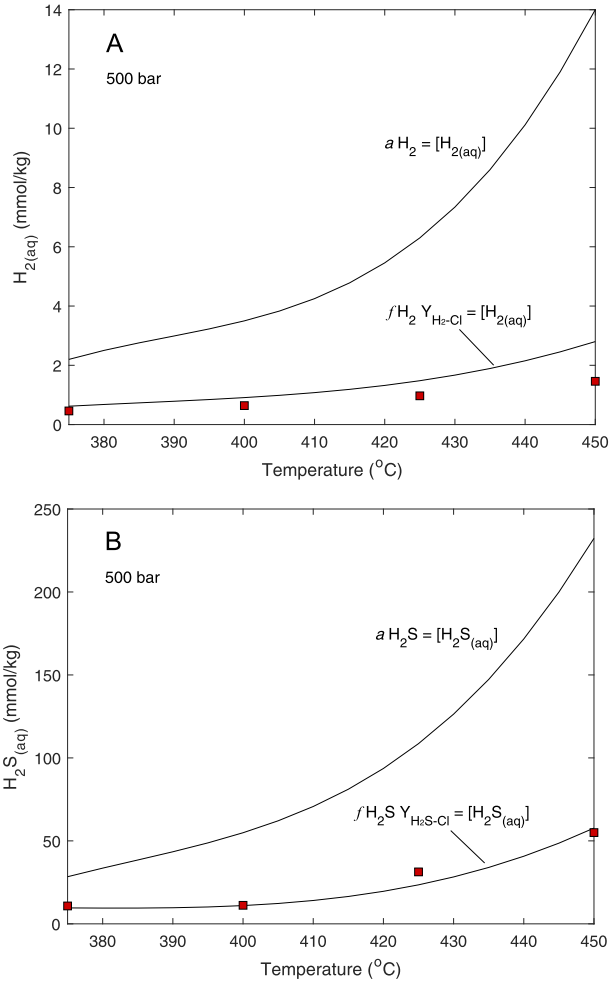

Fig. 8. Comparison of (a) $H_{2(aq)}$ and (b) $H_2S_{(aq)}$ concentrations in equilibrium with pyrite-pyrrhotite-magnetite calculated using two methods: (1) the assumption that concentration is equal to thermodynamic activity as calculated by SUPCRT92 and (2) $Y_{H_2\text{-Cl}}$ and $Y_{H_2S\text{-Cl}}$ values generated using Eqs. (11) and (13), respectively. NaCl concentration for the method 2 calculation is 550 mmol/kg. The red squares represent the experimental data of Ding and Seyfried (1990). Method 1 significantly over predicts dissolved gas concentrations due to uncertainties regarding calculation of Eq. (9) in SUPCT92. The differences between calculation methods 1 and 2 highlight the need for the new experimental data in order to accurately interpret redox conditions of mid-ocean ridge vent fluids.

± 15 °C, 625 ± 30 bar (Scheuermann et al., 2018). The estimated pressure equates to approximately 1.2 km below the seafloor (Scheuermann et al., 2018), a value consistent with geophysical observations of overall crustal thickness, 2–3 km (ten Brink et al., 2002). These pressure–temperature conditions are also consistent with those obtained using a wider suite of geochemical proxies (McDermott et al., 2018). Moreover, the Cu concentrations of the end-member fluids, 127–235 µmol/kg (McDermott et al., 2018), are significantly higher than measured in basalt-seawater laboratory experiments at 400 °C, <30 µmol/kg (Seewald and Seyfried, 1990; Seyfried and Janecky, 1985). Cu is well-known to respond (i.e. precipitate) more quickly than other elements as temperature cools (e.g., Seewald and Seyfried, 1990; Syverson et al., 2017) and therefore its elevated concentration provides further evidence for a deep-seated source of the Piccard vent fluid chemistry (McDermott et al., 2018).

The location of the Piccard field within the axial depression of the Mid-Cayman rise, as well as abundant mafic outcrops and geochemical evidence (e.g., plume CH_4/Mn and high $SiO_{2(aq)}$ in the vent fluid) suggests that the fluid chemistry issuing from Piccard vents is controlled by reaction with mafic lithologies (Stroup and Fox, 1981; German et al., 2010; McDermott et al., 2018). Furthermore, the C isotopic composition of CO_2 (−4.8 to −3.8 ‰, McDermott et al., 2018) suggest mantle input, possibly from active degassing of magma (Kinsey and German, 2013).

However, in contrast to many other systems hosted in mafic volcanic lithologies, the end member $H_{2(aq)}$ concentration, 19.9 mmol/kg, is noteworthy, in that it is greater than that of $H_2S_{(aq)}$, 12 mmol/kg (McDermott et al., 2018). Experimental studies of basalt alteration at temperatures between 300–425 °C indicate that $f\,H_2$ and $f\,H_2S$ are buffered within the range bracketed by the HMP (hematite-magnetite-pyrite) and PPM assemblages (Fig. 9; Seyfried and Ding, 1995; Seyfried et al., 2002). $f\,H_2S$ is larger than $f\,H_2$ as buffered by either HMP or PPM mineral assemblages (Fig. 9), which correspondingly results in $H_2S_{(aq)}$ concentrations greater than $H_{2(aq)}$, since $Y_{H_2S\text{-}Cl}$ is less than $Y_{H_2\text{-}Cl}$ (Fig. 7). Experimentally determined $H_2S_{(aq)}$ concentrations range between 3–20 mmol/kg, while $H_{2(aq)}$ is 0.1–2 mmol/kg (Bischoff and Rosenbauer, 1987; Seewald and Seyfried, 1990; Seyfried et al., 2002; Seyfried et al., 2002). Similar dissolved concentrations of both gases have been measured in natural vent fluids at well-studied, mafic hosted sites such as East Pacific Rise (EPR) 9°N, TAG, and Main Endeavor Field (Von Damm et al., 1985; Humphris and Tivey, 2000; Seyfried et al., 2003; Foustoukos and Seyfried, 2005). Since $Y_{H_2\text{-}Cl}$ is greater than $Y_{H_2S\text{-}Cl}$ (Fig. 7), the observation from the Piccard site ($H_{2(aq)}$ concentration greater than that of $H_2S_{(aq)}$) requires the presence of a mineral assemblage different than either HMP or PPM.

Calculated $f\,H_2$ and $f\,H_2S$ indicate that redox conditions at Piccard are, indeed, well removed from the HMP or PPM triple junctions. At the conditions estimated by the Si-Cl geothermobarometer (540 °C, 625 bar), Eq. (11) yields $Y_{H_2\text{-}Cl}$ of 18 bar/molal. Given the discrepancy between experimental $Y_{H_2\text{-}Cl}$ and predicted Y_{H_2} values at 500 °C (Fig. 5e), it is possible that $Y_{H_2\text{-}Cl}$ may be up to three

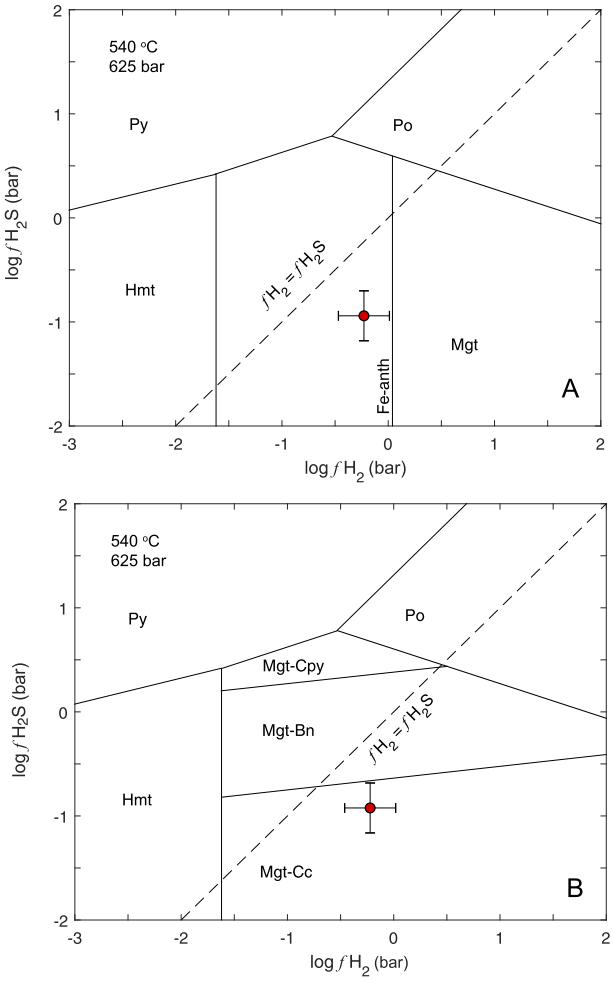

Fig. 9. Phase diagrams displaying the stability fields of redox controlling mineral assemblages in relation to the calculated values of (A) $f\,H_2$ and (B) $f\,H_2S$ (red circles) at the Piccard hydrothermal field. Given the systematics of $Y_{H_2\text{-}Cl}$ and $Y_{H_2S\text{-}Cl}$ and the measured concentrations of $H_{2(aq)}$ and $H_2S_{(aq)}$, redox conditions at Piccard must lie to the right of the $f\,H_2 = f\,H_2S$ boundary. At temperatures greater than 400 °C, the HMP and PPM triple junctions lie to the left of the $f\,H_2 = f\,H_2S$ boundary, thereby distinguishing redox conditions at Piccard from those found in lower temperature basalt-hosted systems. Indeed, $f\,H_2$ at Piccard suggests amphibolite facies alteration and $f\,H_2S$ is consistent with an elevated fluid/rock ratio as compared to many other mafic hosted systems. Mineral abbreviations are py-pyrite, po-pyrrhotite, mgt-magnetite, hmt-hematite, Fe-anth- iron anthophyllite, cpy-chalcopyrite, bn-bornite and cc-chalcocite.

times larger. This uncertainty is accounted for in the error displayed in Fig. 9a and b. Unlike $Y_{H_2\text{-}Cl}$, experimental data for $Y_{H_2S\text{-}Cl}$ reach only to 450 °C and direct calculation of $Y_{H_2S\text{-}Cl}$ (Eq. (13)) at 540 °C, 625 bar results in a $Y_{H_2S\text{-}Cl}$ value of 0.1 bar/molal and a resulting $Y_{H_2\text{-}Cl}/Y_{H_2S\text{-}Cl}$ ratio that is inconsistent with experimental data up to 500 °C (Fig. 7). Instead, $Y_{H_2S\text{-}Cl}$ is estimated based on the value of $Y_{H_2\text{-}Cl}$ and extrapolation of the trend of $Y_{H_2\text{-}Cl}/Y_{H_2S\text{-}Cl}$ taken from Fig. 7. This method yields $Y_{H_2S\text{-}Cl} = 6$ bar/molal. It is important to bear in mind that the estimated subsurface conditions at Piccard require an extrapo-

lation of $Y_{H_2\text{-}Cl}$ and $Y_{H_2S\text{-}Cl}$ of at least 40 °C beyond the range of experimental measurements. While it is difficult to determine exactly the error involved with this extrapolation, the results of Fig. 7 indicate it is unlikely to change the $Y_{H_2\text{-}Cl}/Y_{H_2S\text{-}Cl}$ relationship and therefore $f\ H_2$ remains greater than $f\ H_2S$.

The more reducing nature of Piccard as compared with other basalt-hosted systems may result from the high temperatures that stabilize amphibolite facies mineral assemblages that unlikely at lower temperatures. For example, thermodynamic calculations indicate that the reaction

$$3\ \text{Fe} - \text{anthophyllite} + 4\ H_2O = 7\ \text{Magnetite} + 24\ \text{Quartz} + 7\ H_{2(g)} \quad (14)$$

yields $f\ H_2$ values that are in good agreement with the calculated value at Piccard (Fig. 9a). Thermodynamic data for Fe-anthophyllite ($Fe_7Si_8O_{22}(OH)_2$) come from Holland and Powell (2011), and all other mineral data are from SUPCRT92. While the composition of amphibole solid solutions in nature can depart from that depicted by reaction (14), the general agreement between reaction (14) and Piccard $f\ H_2$ suggests that amphibole solid-solutions are capable of coexisting with high $f\ H_2$ at temperatures exceeding 500 °C. Additionally, assuming an ideal solid-solution mixing model with $Mg_7Si_8O_{22}(OH)_2$, and setting activity of Fe-anthophyllite to 0.1 (0.1 mole fraction Fe) yields log $f\ H_2$ that is 0.5 log units lower than depicted in Fig. 9a. This lower $f\ H_2$ as controlled by Fe-Mg solid solution is within error of our calculation of $f\ H_2$ based on $Y_{H_2\text{-}Cl}$ and measured $H_{2(aq)}$ concentration.

Additionally, given the temperature and pressure conditions likely at Piccard, amphibole minerals are a reasonable alteration assemblage and have been observed in rocks samples recovered from active and fossilized vent systems. Recent drilling at the subaerial basalt-hosted Reykjanes system (Iceland) has shown that amphibolite facies assemblages are pervasive at depths of ~4.5 km (Friðleifsson et al., 2017). Amphibole group minerals have also been observed in sections of fossilized submarine hydrothermal systems at Pito Deep, Hess Deep and ODP Hole 1256 (Coogan et al., 2002; Heft et al., 2008; Alt et al., 2010; Harris et al., 2017). These locations lie within the Eastern Pacific Ocean and are likely representative of modern EPR vents. Interestingly, the active vents at EPR show redox conditions similar to HMP and PPM, as discussed previously. The lack of geochemical evidence in actively venting fluids for amphibolite facies alteration may result from overprinting by fluid-mineral reactions at less extreme conditions during discharge. Due to the depth at which it lies, it is possible the vent fluid chemistry at Piccard preserves the signature of very high temperature alteration processes that also occur in the deepest portion of other mafic hosted vent systems.

Calculated $f\ H_2S$ at Piccard indicates that $H_2S_{(aq)}$ concentrations may be controlled by equilibrium with magnetite-chalcocite ± bornite (Fig. 9b). In basalt-hosted systems, the lack of pyrrhotite or pyrite in the $f\ H_2S$ controlling mineral assemblage requires high fluid/rock ratios in order to render these primary sulfide minerals unstable (Foustoukos and Seyfried, 2005). It is also possible, as suggested by McDermott et al. (2018), that the high fluid/rock ratio prevents saturation of the fluid with respect to any sulfide mineral. Calculations of fluid/rock mass ratios at Piccard yield a range of 2–16, based on vent fluid Li and Rb concentrations, respectively (McDermott et al., 2018). At other mafic hosted systems fluid/rock ratios are generally less than 2 when calculated using Li and Rb (Von Damm et al., 1985; Butterfield and Massoth, 1994; Kadko and Butterfield, 1998). Thus, the unique relationship between $H_{2(aq)}$ and $H_2S_{(aq)}$ concentration at Piccard appears to be the result of the elevated fluid/rock ratio, which lowers $f\ H_2S$, and the extremely high temperature basalt alteration, which produces elevated $f\ H_2$.

5. CONCLUSIONS

Hydrothermal experiments were performed in order to calibrate and evaluate the $f\ H_2$-concentration relationship in saline hydrothermal fluids. Accordingly, $Y_{H_2\text{-}Cl}$ can now be calculated from 300 to 500 °C, 210 to 510 bar in fluids with up to 2000 mmol/kg NaCl or KCl. Similar to the pure water system, $Y_{H_2\text{-}Cl}$ decreases with decreasing fluid density, as the result of changes in pressure, temperature and/or salt concentration. At the conditions investigated, a fluid with 550 mmol/kg NaCl will cause $Y_{H_2\text{-}Cl}$ to be 3–5 times as large as Y_{H_2}. The large deviation of $Y_{H_2\text{-}Cl}$ from Y_{H_2} in fluids of seawater salinity necessitates the use of $Y_{H_2\text{-}Cl}$ in order to accurately calculate the $f\ H_2$ of MOR vent fluids. Application of the new experimental data and previous determination of $Y_{H_2S\text{-}Cl}$ provides improved understanding of high temperature basalt alteration at the Piccard hydrothermal field, Mid-Cayman Rise. Calculated values of $f\ H_2$ are indicative of amphibolite facies alteration, while $f\ H_2S$ suggests an elevated fluid/rock ratio, consistent with dissolved Li and Rb concentrations. While amphibole group minerals are common in rock samples recovered from both active (Reykjanes, Iceland) and fossilized (e.g., Pito Deep) mafic hosted vent systems, fluids from most modern systems do not maintain the geochemical signature of these high temperature reactions. Piccard may be the first active system to provide a previously unavailable window into high temperature (>500 °C) hydrothermal alteration processes likely typical of deeper zones of mafic-hosted MOR systems in general.

ACKNOWLEDGEMENTS

We thank Liz Lundstrom for analytical support. The authors also gratefully acknowledge funding provided by NSF grant OCE # 1426695 (WES). This manuscript benefited greatly from constructive comments provided by the Associate Editor, Frieder Klein, and four anonymous reviewers.

APPENDIX A

Ding and Seyfried (1990) experimental and analytical procedures

The experiments of Ding and Seyfried (1990) were performed in gold cell hydrothermal reactors (Seyfried et al.,

1987) at the pressures and temperatures indicated in Table 2. Fluid samples were collected using procedures described in Seyfried et al. (1987) and Seewald and Seyfried (1990). In order to accurately measure both $H_{2(aq)}$ and $H_2S_{(aq)}$ concentrations a quick quench method was used (e.g., Seewald and Seyfried, 1990; Foustoukos and Seyfried, 2005). Fluid-mineral equilibria was assessed using the same methods described in this study.

The analytical techniques have been described by Seewald and Seyfried (1990). Analytical uncertainty (2σ) for dissolved ionic species is 2% and 5% for $H_{2(aq)}$ and $H_2S_{(aq)}$ (see Figs. A1–A5 and Table A1).

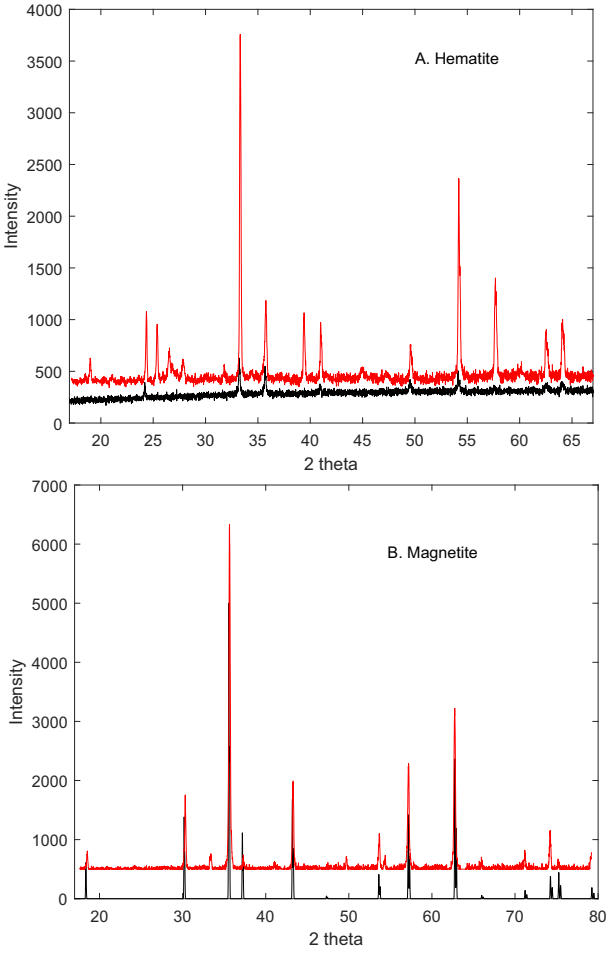

Fig. A1. Comparison of XRD spectra from the minerals used in the present study with those in the RRUFF online database. In each image the red spectra represent the spectra taken after the experiment and the black spectra are from the RRUFF database. The sample numbers from the RRUFF database are: Magnetite R061111, Hematite R040024. The increase in wt% K_2O, Al_2O_3, and SiO_2 between the pre- and post-experiment hematite suggests incorporation of either K-feldspar or muscovite in the post-experiment hematite sample. The exact mineral is difficult to determine through Rietveld fitting of XRD data due to the low-intensity of the peaks and overlapping peaks between K-feldspar and muscovite.

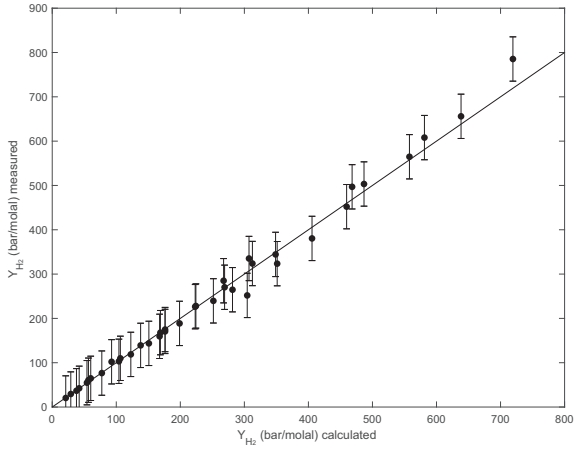

Fig. A2. Comparison of measured and calculated Y_{H_2} values. Measured values correspond to the experimental data of Kishima and Sakai (1984a,b), while calculated values are from Eq. (10). The black line represents equivalence. Error bars represent ±50 bar/molal.

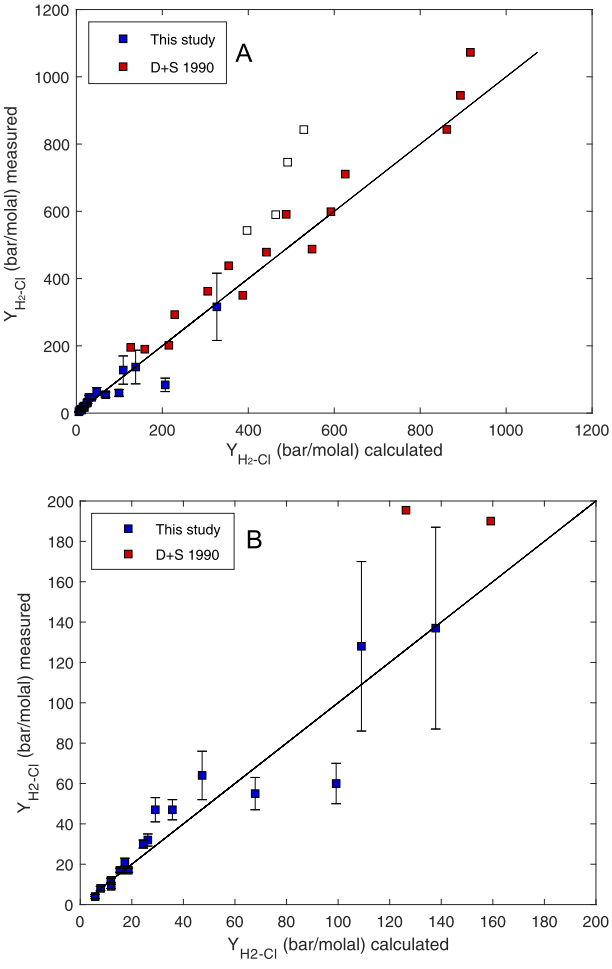

Fig. A3. Comparison of measured and calculated $Y_{H_2\text{-}Cl}$ values. Measured values correspond to the experimental data generated in this study and Ding and Seyfried (1990), while calculated values are from Eq. (11). Empty squares represent samples with NaCl greater than 1000 mmol/kg. The black lines represent equivalence. Panel B shows the same data as A, but over a smaller range of values.

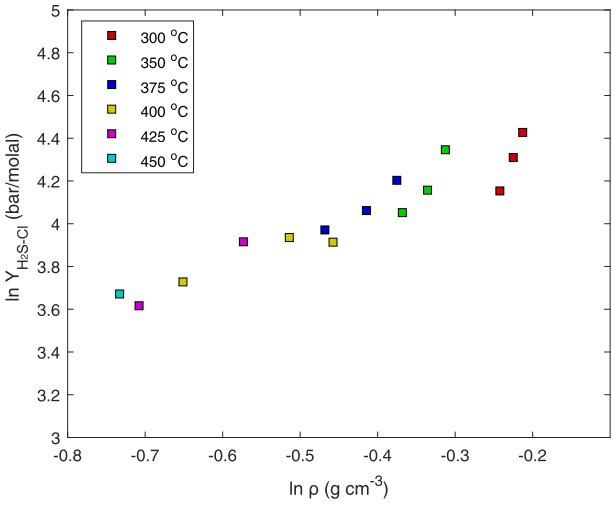

Fig. A4. ln $Y_{H_2S\text{-}Cl}$ as a function of ln ρ. Experimental data are from Ding and Seyfried (1990).

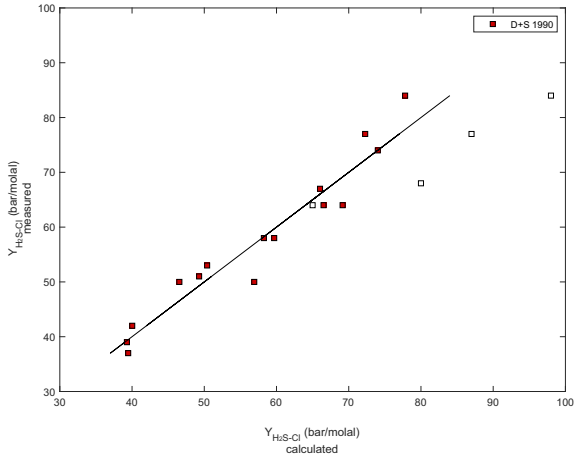

Fig. A5. Comparison of measured and calculated $Y_{H_2S\text{-}Cl}$ values. Measured values correspond to the experimental data of Ding and Seyfried (1990). Calculated values are from Eq. (13). The black line represent equivalence. Empty squares represent samples with NaCl concentrations greater than 1000 mmol/kg.

Table A1
Chemical composition of minerals.

	Al_2O_3 wt%	CaO wt%	Fe_2O_{3T} wt%	K_2O wt%	MgO wt%	MnO wt%	Na_2O wt%	P_2O_5 wt%	SiO_2 wt%	TiO_2 wt%	total wt%
Magnetite	0.37	0.01	90.53	0.11	0.23	0.03	3.07	0.04	2.22	0.04	96.65
	0.35	**0.22**	**84.75**	**0.21**	**0.25**	**0.03**	**3.08**	**0.15**	**2.60**	**0.03**	**91.68**
Hematite	2.81	0.02	79.91	0.10	0.12	0.12	3.00	0.04	6.38	0.90	93.40
	4.58	**0.19**	**70.91**	**1.41**	**0.81**	**0.20**	**2.68**	**0.26**	**11.18**	**0.85**	**93.07**

Values reported are the average of three measurements.
Values in plain text represent analysis pre-experiment. Bold text represents analysis after the experiment.

APPENDIX B. SUPPLEMENTARY MATERIAL

Supplementary data to this article can be found online at https://doi.org/10.1016/j.gca.2020.05.020.

REFERENCES

Akinfiev N. N. and Diamond L. W. (2003) Thermodynamic description of aqueous nonelectrolytes at infinite dilution over a wide range of state parameters. *Geochim. Cosmochim. Acta* **67**, 613–629.

Alt J. C., Laverne C., Coggon R. M., Teagle D. A. H., Banerjee N. R., Morgan S., Smith-Duque C. E., Harris M. and Galli L. (2010) Subsurface structure of a submarine hydrothermal system in ocean crust formed at the East Pacific Rise, ODP/IODP Site 1256. *Geochem. Geophys. Geosyst.* **11**.

Anderson G. M. and Crerar D. A. (1993) *Thermodynamics in Geochemistry: The Equilibrium Model*. Oxford University Press, New York, NY.

Anderson R. E., Reveillaud J., Reddington E., Delmont T. O., Eren A. M., McDermott J. M., Seewald J. S. and Huber J. A. (2017) Genomic variation in microbial populations inhabiting the marine subseafloor at deep-sea hydrothermal vents. *Nat. Commun.* **8**, 1114.

Barton P. and Skinner B. (1979) Sulfide mineral stabilities. In *Geochemistry of Hydrothermal Ore Deposits*. John Wiley & Sons, New, York, pp. 278–390.

Bischoff J. L. and Rosenbauer R. J. (1987) Phase separation in seafloor geothermal systems; an experimental study of the effects on metal transport. *Am. J. Sci.* **287**, 953–978.

Bodnar R. J. and Sterner S. M. (1985) Synthetic fluid inclusions in natural quartz. II. Application to PVT studies. *Geochim. Cosmochim. Acta* **49**, 1855–1859.

ten Brink U. S., Coleman D. F. and Dillon W. P. (2002) The nature of the crust under Cayman Trough from gravity. *Mar. Pet. Geol.* **19**, 971–987.

Butterfield D. A. and Massoth G. J. (1994) Geochemistry of north Cleft segment vent fluids: Temporal changes in chlorinity and their possible relation to recent volcanism. *J. Geophys. Res.* **99**, 4951–4968.

Charlou J. L., Donval J. P., Fouquet Y., Jean-Baptiste P. and Holm N. (2002) Geochemistry of high H_2 and CH_4 vent fluids issuing from ultramafic rocks at the Rainbow hydrothermal field (36°14′N, MAR). *Chem. Geol.* **191**, 345–359.

Chou I.-M. (1978) Calibration of oxygen buffers at elevated P and T using the hydrogen fugacity sensor. *Am. Mineral.* **63**, 690–703.

Connelly D. P., Copley J. T., Murton B. J., Stansfield K., Tyler P. A., German C. R., Dover C. L. V., Amon D., Furlong M., Grindlay N., Hayman N., Hühnerbach V., Judge M., Bas T. L., McPhail S., Meier A., Nakamura K., Nye V., Pebody M., Pedersen R. B., Plouviez S., Sands C., Searle R. C., Stevenson P., Taws S. and Wilcox S. (2012) Hydrothermal vent fields and chemosynthetic biota on the world's deepest seafloor spreading centre. *Nat. Commun.* **3**.

Coogan L. A., Gillis K. M., MacLeod C. J., Thompson G. M. and Hékinian R. (2002) Petrology and geochemistry of the lower ocean crust formed at the East Pacific Rise and exposed at Hess Deep: A synthesis and new results. *Geochem. Geophys. Geosyst.* **3**, 8604.

Ding, K., Seyfried, W.E., 1990. Activity coefficients of H_2 and H_2S in NaCl solutions at 300-450C, 300-500 bars with applications to ridge crest hydrothermal systems. In: EOS American Geophysical Union. p. 1680.

Ding K. and Seyfried W. E. (1992) Determination of Fe-Cl complexing in the low pressure supercritical region (NaCl fluid): Iron solubility constraints on pH of subseafloor hydrothermal fluids. *Geochim. Cosmochim. Acta* **56**, 3681–3692.

Driesner T. (2007) The system H_2O–NaCl. Part II: Correlations for molar volume, enthalpy, and isobaric heat capacity from 0 to 1000 °C, 1 to 5000 bar, and 0 to 1 XNaCl. *Geochim. Cosmochim. Acta* **71**, 4902–4919.

Driesner T. and Heinrich C. A. (2007) The system H_2O–NaCl. Part I: Correlation formulae for phase relations in temperature–pressure–composition space from 0 to 1000 °C, 0 to 5000 bar, and 0 to 1 XNaCl. *Geochim. Cosmochim. Acta* **71**, 4880–4901.

Drummond E. (1981) *Boiling and mixing of hydrothermal fluids: Chemical effects on mineral precipitation* PhD. Pennsylvania State University.

Eklund K., Lvov S. N. and Macdonald D. D. (1997) The measurement of Henry's constant for hydrogen in high subcritical and supercritical aqueous systems. *J. Electroanal. Chem.* **437**, 99–110.

Foustoukos D. I. and Seyfried W. E. (2005) Redox and pH constraints in the subseafloor root zone of the TAG hydrothermal system, 26° N Mid-Atlantic Ridge. *Earth Planet. Sci. Lett.* **235**, 497–510.

Foustoukos D. and Seyfried W. (2007) Fluid phase separation processes in submarine hydrothermal systems. In *Fluid-Fluid Interactions. Reviews in Mineralogy and Geochemistry* (eds. A. Liebscher and C. Heinrich). Mineralogical Society of America, Geochemical Society.

Fowler A. P. G., Scheuermann P., Tan C. and Seyfried W. (2019) Titanium reactors for redox-sensitive hydrothermal experiments: An assessment of dissolved salt on H_2 activity-concentration relations. *Chem. Geol.* **515**, 87–93.

Friðleifsson G. Ó., Elders W. A., Zierenberg R. A., Stefánsson A., Fowler A. P. G., Weisenberger T. B., Harðarson B. S. and Mesfin K. G. (2017) The Iceland Deep Drilling Project 4.5 km deep well, IDDP-2, in the seawater-recharged Reykjanes geothermal field in SW Iceland has successfully reached its supercritical target. *Sci. Drill.* **23**, 1–12.

Gallant R. M. and Von Damm K. L. (2006) Geochemical controls on hydrothermal fluids from the Kairei and Edmond Vent Fields, 23°–25°S Central Indian Ridge. *Geochem. Geophys. Geosyst.* **7**, Q06018.

German C. R., Bowen A., Coleman M. L., Honig D. L., Huber J. A., Jakuba M. V., Kinsey J. C., Kurz M. D., Leroy S., McDermott J. M., de Lépinay B. M., Nakamura K., Seewald J. S., Smith J. L., Sylva S. P., Van Dover C. L., Whitcomb L. L. and Yoerger D. R. (2010) Diverse styles of submarine venting on the ultraslow spreading Mid-Cayman Rise. *Proc. Natl. Acad. Sci. U. S. A.* **107**, 14020–14025.

German C. R. and Seyfried W. E. (2014) Hydrothermal processes. In *Treatise on Geochemistry* (eds. H. D. Holland and K. K. Turekian), second ed. Elsevier, Oxford, pp. 191–233.

Harris M., Coggon R. M., Wood M., Smith-Duque C. E., Henstock T. J. and Teagle D. A. H. (2017) Hydrothermal cooling of the ocean crust: Insights from ODP Hole 1256D. *Earth Planet. Sci. Lett.* **462**, 110–121.

Heft K. L., Gillis K. M., Pollock M. A., Karson J. A. and Klein E. M. (2008) Role of upwelling hydrothermal fluids in the development of alteration patterns at fast spreading ridges: Evidence from the sheeted dike complex at Pito Deep. *Geochem. Geophys. Geosyst.* **9**.

Holland T. J. B. and Powell R. (2011) An improved and extended internally consistent thermodynamic dataset for phases of petrological interest, involving a new equation of state for solids. *J. Metamorph. Geol.* **29**, 333–383.

Holland T. J. B. and Powell R. (1998) An internally consistent thermodynamic data set for phases of petrological interest. *J. Metamorph. Geol.* **16**, 309–343.

Humphris S. E. and Tivey M. K. (2000) A synthesis of geological and geochemical investigations of the TAG hydrothermal field: Insights into fluid-flow and mixing processes in a hydrothermal system. In *Special Paper 349: Ophiolites and Oceanic Crust: New Insights from Field Studies and the Ocean Drilling Program*. Geological Society of America, pp. 213–235.

Japas M. L. and Sengers J. M. H. L. (1989) Gas solubility and Henry's law near the solvent's critical point. *AIChE J.* **35**, 705–713.

Johnson, Oelkers and Helgeson (1992) SUPCRT92: A software package for calculationg the standard molal thermodynamic properties of minerals, gases, aqueous species and reactions from 1 to 500 bar and 0 to 1000 C. *Comput. Geosci.* **18**, 899–947.

Kadko D. and Butterfield D. A. (1998) The relationship of hydrothermal fluid composition and crustal residence time to maturity of vent fields on the Juan de Fuca Ridge. *Geochim. Cosmochim. Acta* **62**, 1521–1533.

Khaibullin K. and Borisov N. M. (1966) Experimental investigation of the thermal properties of aqueous and vapour solutions of sodium and potassium chloride at phase equilibrium. *High Temp.* **4**, 489–494.

Kinsey J. C. and German C. R. (2013) Sustained volcanically-hosted venting at ultraslow ridges: Piccard Hydrothermal Field, Mid-Cayman Rise. *Earth Planet. Sci. Lett.* **380**, 162–168.

Kishima N. (1989) A thermodynamic study on the pyrite-pyrrhotite-magnetite-water system at 300–500°C with relevance to the fugacity/concentration quotient of aqueous H_2S. *Geochim. Cosmochim. Acta* **53**, 2143–2155.

Kishima N. and Sakai H. (1984a) Fugacity-concentration relationship of dilute hydrogen in water at elevated temperature and pressure. *Earth Planet. Sci. Lett.* **67**, 79–86.

Kishima N. and Sakai H. (1984b) A simple gas analytical technique for the Dickson-type hydrothermal apparatus and its application to the calibration of MH, NNO and FMQ oxygen buffers. *Geochem. J.* **18**, 19–29.

Klein F., Bach W., Jöns N., McCollom T., Moskowitz B. and Berquó T. (2009) Iron partitioning and hydrogen generation during serpentinization of abyssal peridotites from 15°N on the Mid-Atlantic Ridge. *Geochim. Cosmochim. Acta* **73**, 6868–6893.

Klein F., Bach W. and McCollom T. M. (2013) Compositional controls on hydrogen generation during serpentinization of ultramafic rocks. *Lithos* **178**, 55–69.

Liebscher A. (2007) Experimental studies in model fluid systems. In *Fluid-Fluid Interactions. Reviews in Mineralogy and Geochemistry* (eds. A. Liebscher and C. A. Heinrich). Mineralogical Society of America. Geochemical Society, pp. 15–47.

Lilley M. D., Butterfield D. A., Lupton J. E. and Olson E. J. (2003) Magmatic events can produce rapid changes in hydrothermal vent chemistry. *Nature* **422**, 878–881.

McCollom T. M. and Seewald J. S. (2003) Experimental constraints on the hydrothermal reactivity of organic acids and acid anions: I. Formic acid and formate. *Geochim. Cosmochim. Acta* **67**, 3625–3644.

McCollom T. M. and Shock E. L. (1998) Fluid-rock interactions in the lower oceanic crust: Thermodynamic models of hydrothermal alteration. *J. Geophys. Res.* **103**, 547–575.

McDermott J. M., Sylva S. P., Ono S., German C. R. and Seewald J. S. (2018) Geochemistry of fluids from Earth's deepest ridge-crest hot-springs: Piccard hydrothermal field, Mid-Cayman Rise. *Geochim. Cosmochim. Acta* **228**, 95–118.

Oelkers E. H. and Helgeson H. C. (1991) Calculation of activity coefficients and degrees of formation of neutral ion pairs in supercritical electrolyte solutions. *Geochim. Cosmochim. Acta* **55**, 1235–1251.

Pester N. J., Ding K. and Seyfried, Jr., W. E. (2015) Vapor–liquid partitioning of alkaline earth and transition metals in NaCl-dominated hydrothermal fluids: An experimental study from 360 to 465 °C, near-critical to halite saturated conditions. *Geochim. Cosmochim. Acta* **168**, 111–132.

Plyasunov A. V., O'Connell J. P. and Wood R. H. (2000) Infinite dilution partial molar properties of aqueous solutions of nonelectrolytes. I. Equations for partial molar volumes at infinite dilution and standard thermodynamic functions of hydration of volatile nonelectrolytes over wide ranges of conditions. *Geochim. Cosmochim. Acta* **64**, 495–512.

Scheuermann P. P., Tan C. and Seyfried W. E. (2018) Quartz solubility in the two-phase region of the NaCl-H_2O system: an experimental study with application to the Piccard hydrothermal field, mid-Cayman rise. *Geochem. Geophys. Geosyst.* **19**, 3570–3582.

Scheuermann P. P., Tutolo B. M. and Seyfried W. E. (2019) Anhydrite solubility in low-density hydrothermal fluids: Experimental measurements and thermodynamic calculations. *Chem. Geol.* **524**, 184–195.

Schmidt K., Koschinsky A., Garbe-Schönberg D., de Carvalho L. M. and Seifert R. (2007) Geochemistry of hydrothermal fluids from the ultramafic-hosted Logatchev hydrothermal field, 15°N on the Mid-Atlantic Ridge: Temporal and spatial investigation. *Chem. Geol.* **242**, 1–21.

Seewald J., Cruse A. and Saccocia P. (2003) Aqueous volatiles in hydrothermal fluids from the Main Endeavour Field, northern Juan de Fuca Ridge: temporal variability following earthquake activity. *Earth Planet. Sci. Lett.* **216**, 575–590.

Seewald J. S. and Seyfried W. E. (1990) The effect of temperature on metal mobility in subseafloor hydrothermal systems: constraints from basalt alteration experiments. *Earth Planet. Sci. Lett.* **101**, 388–403.

Seyfried W. E. and Janecky D. R. (1985) Heavy metal and sulfur transport during subcritical and supercritical hydrothermal alteration of basalt: Influence of fluid pressure and basalt composition and crystallinity. *Geochim. Cosmochim. Acta* **49**, 2545–2560.

Seyfried W. E. and Ding K. (1995) Phase equilibria in subseafloor hydrothermal systems: a review of the role of redox, temperature, Ph and dissolved Cl on the chemistry of hot spring fluids at Mid-Ocean Ridges. In *Geophysical Monograph Series* (eds. S. E. Humphris, R. A. Zierenberg, L. S. Mullineaux and R. E. Thomson). American Geophysical Union, Washington, D. C., pp. 248–272.

Seyfried W. E., Ding K. and Rao B. (2002) Experimental calibration of metastable plagioclase-epidote-fluid equilibria at elevated temperatures and pressures: Applications to the chemistry of hydrothermal fluids at mid-oceans ridges. In *Water-Rock Interactions, Ore Deposits, and Environmental Geochemistry: A Tribute to David A. Crerar* (eds. R. Hellman and S. A. Wood). The Geochemical Society, pp. 257–278.

Seyfried W. E., Janecky D. R. and Berndt M. E. (1987) Rocking autoclaves for hydrothermal experiments II: The flexible cell system. In *Experimental Hydrothermal Techniques* (eds. G. Ulmer and H. Barnes). Wiley Interscience, pp. 216–240.

Seyfried W. E., Pester N. J., Ding K. and Rough M. (2011) Vent fluid chemistry of the Rainbow hydrothermal system (36°N, MAR): Phase equilibria and in situ pH controls on subseafloor alteration processes. *Geochim. Cosmochim. Acta* **75**, 1574–1593.

Seyfried W. E., Seewald J. S., Berndt M. E., Ding K. and Foustoukos D. I. (2003) Chemistry of hydrothermal vent fluids from the Main Endeavour Field, northern Juan de Fuca Ridge: Geochemical controls in the aftermath of June 1999 seismic events. *J. Geophys. Res.* **108**, 2429.

Seyfried W. E., Pester N. J., Tutolo B. M. and Ding K. (2015) The Lost City Hydrothermal system: Constraints imposed by vent fluid chemistry and reaction path models on subseafloor heat and mass transfer processes. *Geochim. Cosmochim. Acta* **163**, 59–79.

Sharygin A. V., Wood R. H., Zimmerman G. H. and Balashov V. N. (2002) Multiple ion association versus redissociation in aqueous NaCl and KCl at high temperatures. *J. Phys. Chem. B* **106**, 7121–7134.

Shock E. L. and Helgeson H. C. (1988) Calculation of the thermodynamic and transport properties of aqueous species at high pressures and temperatures: Correlation algorithms for ionic species and equation of state predictions to 5 kb and 1000° C. *Geochim. Cosmochim. Acta* **52**, 2009–2036.

Shock E. L. and Helgeson H. C. (1990) Calculation of the thermodynamic and transport properties of aqueous species at high pressures and temperatures: Standard partial molal properties of organic species. *Geochim. Cosmochim. Acta* **54**, 915–945.

Shock E. L., Helgeson H. C. and Sverjensky D. A. (1989) Calculation of the thermodynamic and transport properties of aqueous species at high pressures and temperatures: Standard partial molal properties of inorganic neutral species. *Geochim. Cosmochim. Acta* **53**, 2157–2183.

Stroup J. B. and Fox P. J. (1981) Geologic investigations in the Cayman Trough: evidence for thin oceanic crust along the Mid-Cayman Rise. *J. Geol.* **89**, 395–420.

Syverson D. D., Luhmann A. J., Tan C., Borrok D. M., Ding K. and Seyfried, Jr., W. E. (2017) Fe isotope fractionation between chalcopyrite and dissolved Fe during hydrothermal recrystallization: An experimental study at 350 °C and 500 bars. *Geochim. Cosmochim. Acta* **200**, 87–109.

Tanger J. C. and Helgeson H. C. (1988) Calculation of the thermodynamic and transport properties of aqueous species at high pressures and temperatures; revised equations of state for the standard partial molal properties of ions and electrolytes. *Am. J. Sci.* **288**, 19–98.

Von Damm K. L. (2000) Chemistry of hydrothermal vent fluids from 9°–10°N, East Pacific Rise: "Time zero", the immediate posteruptive period. *J. Geophys. Res.* **105**, 11203–11222.

Von Damm K. L. (1995) Controls on the chemistry and temporal variability of seafloor hydrothermal fluids. In *Seafloor Hydrothermal Systems: Physical, Chemical, Biological, and Geological Interactions*, pp. 222–247.

Von Damm K. L. (1990) Seafloor hydrothermal activity: black smoker chemistry and chimneys. *Annu. Rev. Earth Planet. Sci.* **18**, 173–204.

Von Damm K. L., Edmond J. M., Grant B., Measures C. I., Walden B. and Weiss R. F. (1985) Chemistry of submarine hydrothermal solutions at 21 °N, East Pacific Rise. *Geochim. Cosmochim. Acta* **49**, 2197–2220.

Von Damm K. L., Lilley M. D., Shanks, III, W. C., Brockington M., Bray A. M., O'Grady K. M., Olson E., Graham A. and Proskurowski G. (2003) Extraordinary phase separation and segregation in vent fluids from the southern East Pacific Rise. *Earth Planet. Sci. Lett.* **206**, 365–378.

Von Damm K. L. V., Oosting S. E., Kozlowski R., Buttermore L. G., Colodner D. C., Edmonds H. N., Edmond J. M. and Grebmeier J. M. (1995) Evolution of East Pacific Rise hydrothermal vent fluids following a volcanic eruption. *Nature* **375**, 47–50.

Associate editor: Frieder Klein